

# MODELS OF THE ICM WITH HEATING AND COOLING: EXPLAINING THE GLOBAL AND STRUCTURAL X-RAY PROPERTIES OF CLUSTERS

IAN G. MCCARTHY<sup>1</sup>, MICHAEL L. BALOGH<sup>2,3</sup>, ARIF BABUL<sup>1</sup>, GREGORY B. POOLE<sup>1</sup>, AND DONALD J. HORNER<sup>4</sup>

<sup>1</sup>Department of Physics & Astronomy, University of Victoria, Victoria, BC, V8P 1A1, Canada; mcarthy@uvastro.phys.uvic.ca, babul@uvic.ca, gbpoole@uvastro.phys.uvic.ca

<sup>2</sup>Department of Physics, University of Durham, Durham, DH1 3LE, UK; m.l.balogh@durham.ac.uk

<sup>3</sup>Present address: Department of Physics, University of Waterloo, Waterloo, ON, N2L 3G1, Canada and

<sup>4</sup>Department of Astronomy, University of Massachusetts, Amherst, MA 01003; horner@astro.umass.edu

*To appear in the Astrophysical Journal (received 03/05/04, accepted 06/10/04)*

## ABSTRACT

Non-radiative simulations which only include heating due to gravitational processes fail to match the observed mean X-ray properties of galaxy clusters. As a result, there has recently been increased interest in models in which either radiative cooling or entropy injection (and/or redistribution) play a central role in mediating the thermal and spatial properties of the intracluster medium. Both sets of models can account for the mean global properties of clusters. Radiative cooling alone, however, results in fractions of cold/cooled baryons in excess of observationally established limits. On the other hand, the simplest entropy injection models, by design, do not treat the “cooling core” structure present in many clusters and cannot account for declining entropy profiles towards cluster centers revealed by recent high resolution X-ray observations. We consider models that marry radiative cooling with entropy injection, and confront model predictions for the global and structural properties of massive clusters with the latest X-ray data. The models successfully and simultaneously reproduce the observed  $L - T$  and  $L - M$  relations, yield detailed entropy, surface brightness, and temperature profiles in excellent agreement with observations, and predict a cooled gas fraction that is consistent with observational constraints. More interestingly, the model provides a possible explanation for the significant intrinsic scatter present in the  $L - T$  and  $L - M$  relations. The model also offers a natural way of distinguishing between clusters classically identified as “cooling flow” clusters and the relaxed “non-cooling flow” clusters. The former correspond to systems that experienced only mild levels ( $\lesssim 300 \text{ keV cm}^2$ ) of entropy injection, while the latter are identified as systems that had much higher entropy injection. The dividing line in entropy injection between the two categories corresponds roughly to the cooling threshold for massive clusters. This finding suggests that entropy injection may be an important, if not the primary, factor in determining the class a particular cluster will belong to. These results also suggest that the previously identified relationship between inferred cooling flow strength and the dispersion in the  $L - T$  relation is a manifestation of the distribution of cluster entropy injection levels. This is borne out by the entropy profiles derived from *Chandra* and *XMM-Newton*. Finally, the model predicts a relationship between a cluster’s central entropy and its core radius, the existence of which we confirm in the observational data.

*Subject headings:* cosmology: theory — galaxies: clusters: general — X-rays: galaxies: clusters

## 1. INTRODUCTION

It has been made increasingly apparent in recent years that theoretical models of cluster formation and evolution that incorporate gravitationally-driven processes alone fail to match the observed global X-ray properties of clusters (e.g., Kaiser 1991, Tozzi & Norman 2001; Babul et al. 2002). More recently, McCarthy et al. (2003a, 2003b) showed that such models are also incompatible with the observed Sunyaev-Zeldovich (SZ) effect properties of distant clusters. This discord between theory and observations has motivated a number of authors to examine the potential role of *non*-gravitational gas physics, usually in the form of radiative cooling, entropy injection<sup>5</sup> (e.g., from AGN or galactic winds), or both cooling and entropy injection (e.g., Kaiser 1991; Balogh, Babul, & Patton 1999; Bryan 2000; Tozzi & Norman 2001; Borgani et al. 2001; Voit & Bryan 2001; Babul et al. 2002; Wu & Xue 2002; Voit et al. 2002; Davé, Katz, & Weinberg 2002; Voit et al. 2003; Oh & Benson 2003). These models generally compare more favorably

to the data [e.g., to the observed luminosity-temperature ( $L - T$ ) and luminosity-mass ( $L - M$ ) relations] than the standard ‘non-radiative’ model, but it still remains somewhat unclear as to which of these models — those with entropy injection alone, those with cooling alone, or those with entropy injection plus cooling — best reflect the true nature of clusters.

Part of the reason for the ambiguity undoubtedly arises from the fact that there is a relatively large amount of scatter present in the observed X-ray scaling relations of clusters, in particular the  $L - T$  and  $L - M$  relations. Because of the large scatter, the various non-gravitational models, which typically predict similar mean global properties, are essentially indistinguishable (see, e.g., Voit et al. 2002; Balogh et al. 2004).

<sup>5</sup> We also regard mechanisms such as thermal conduction and turbulent mixing (e.g., Narayan & Medvedev 2001; Kim & Narayan 2003) as sources of ‘entropy injection’ since they transfer heat to the cluster center. Strictly speaking, however, these processes do not really introduce new entropy into the system, they merely *redistribute* the cluster’s (pre-existing) entropy.

The origin of the scatter in the observed relations is uncertain and has received very little attention from a theoretical modeling point of view. It is clear that at least some of the dispersion is due to real physical differences in the properties of clusters of a given mass (as the observed scatter cannot be explained by measurement uncertainty) and, therefore, any realistic theoretical model of cluster evolution that seeks to make precise predictions must account for it. Understanding the origin of the scatter is of considerable importance to studies seeking to use clusters for precision cosmological tests, such as the determination of the matter power spectrum normalization,  $\sigma_8$  (see, e.g., Smith et al. 2003; Balogh et al. 2004).

An examination of whether or not the intrinsic scatter can be accounted for by non-gravitational gas physics, therefore, is one of the primary goals of the present paper. We demonstrate below that *the scatter in the  $L-T$  and  $L-M$  relations is inconsistent with entropy injection only or cooling only models*. However, the scatter can be accounted for by a model that includes both entropy injection and radiative cooling. Moreover, our analysis indicates variations in the efficiency of entropy injection across the cluster population. Combined cooling + entropy injection models also have the advantage of not being subject to the “overcooling” problems that plague the purely radiative cooling models.

While detailed studies of the global properties of clusters have taught us much (and continue to teach us) about the intracluster medium (ICM) and clusters in general, a potentially much more powerful test is comparisons between observed and predicted *structural* properties, such as entropy, temperature, and surface brightness profiles. The influx of new high spatial and high spectral resolution X-ray data from *Chandra* and *XMM-Newton* now affords us the opportunity to make such comparisons. A second goal of this study, therefore, is to confront theoretical models that include entropy injection and/or cooling with new high resolution data. We note that early results from *Chandra* and *XMM-Newton* show no signs of the large isentropic cores in groups and clusters predicted by generic injection only models (e.g., David et al. 2001; Pratt & Arnaud 2003; Mushotzky et al. 2003). This implies that other processes, possibly radiative cooling, are also important, at least for some clusters. Indeed, we demonstrate that models with both radiative cooling and entropy injection are able to match the observed structural properties of massive clusters and simultaneously account for the  $L-T$  and  $L-M$  relations. Interestingly, the theoretical systems with only mild levels of entropy injection look remarkably like “cooling flow” (CF) clusters<sup>6</sup>, whereas systems with high levels exhibit the typical characteristics of “non-cooling flow” (NCF) clusters.

The present paper is organized as follows. In §2, we

extend the models of Babul et al. (2002) to include a realistic treatment of radiative cooling. A general discussion of how radiative cooling modifies the properties of the models is given in §3. In §4, the physical origin of the scatter in the  $L-T$  and  $L-M$  relations is explored. Comparisons of structural properties between the various theoretical models and high quality *Chandra* and *XMM-Newton* data are made in §5. Finally, in §6 and §7, we summarize and discuss our results.

The models considered below were developed in a flat  $\Lambda$ CDM cosmology with  $h = 0.75$ ,  $\Omega_m = 0.3$  and  $\Omega_b = 0.020h^{-2}$ , which is a close match to current estimates, including those from *WMAP* (Spergel et al. 2003).

## 2. CLUSTER MODELS WITH RADIATIVE COOLING

The primary goal of this paper is to explore how entropy injection and radiative cooling influence the evolution of the ICM and to confront these models with new high quality X-ray data. We have already performed a thorough analysis of how entropy injection alone modifies the ICM (e.g., Balogh, Babul, & Patton 1999; Babul et al. 2002; McCarthy et al. 2002a, 2003a, 2003b, 2003c). This model sought to explain the properties of groups and clusters *minus* the “cooling flow” component, if any, and therefore, explicitly ignored radiative cooling. We refer the reader to Babul et al. (2002), in particular, for an in-depth discussion of the model, including an examination of the possible sources of the entropy injection. We re-examine the issue of sources of non-gravitational entropy in §6 of the present paper.

Since we have examined the effects of entropy injection in detail, the current section is devoted to an examination of the effects of radiative cooling. First, however, a short discussion of the initial conditions prior to cooling is given so that we may gauge how cooling modifies things.

### 2.1. Initial conditions

There have been claims that radiative cooling alone may explain the deviations of clusters from self-similarity (e.g., Bryan 2000; Wu & Xue 2002; Davé, Katz, & Weinberg 2002) or, at least, that it plays the dominant role in the breaking of self-similarity (e.g., Voit & Ponman 2003). In order to explore this possibility, we examine the effects of cooling on the simple isothermal model of Babul et al. (2002). As its name implies, this isothermal model assumes that initially (i.e., before any cooling) the ICM has a constant temperature, which is set to the cluster virial temperature. The intracluster gas is in hydrostatic equilibrium within a gravitationally-dominant dark matter halo that has a density profile which matches those found in recent high resolution numerical simulations (e.g., Moore et al. 1999; Lewis et al. 2000). In order to solve for hydrostatic equilibrium, it is assumed that the cluster is a typical region of the universe in terms of the mixture of dark matter and baryons, i.e., the ratio of gas mass to total mass within cluster’s maximum radius,  $r_{\text{halo}}$ , is given by  $\Omega_b/\Omega_m$ . In terms of global properties, this simple model has been shown to be in excellent agreement with self-similar predictions (i.e., it predicts  $L \propto T^2$  and  $L \propto M^{4/3}$ ) and with the results of non-radiative simulations, such as those performed by Evrard, Metzler, & Navarro (1996). The simplicity of this model makes it particularly suitable for analysis.

<sup>6</sup> The designation “cooling flow” cluster refers to a system that has a sharply rising surface brightness profile and, normally, a declining temperature profile towards the center. These observational characteristics have typically been interpreted as manifestations of an ICM that is radiatively cooling on short timescales. The cooling gas flows inward toward the cluster center (hence, the name cooling flow). When we use the phrase “cooling flow” (in quotation marks) we are referring to the observational characteristics and not a physical model.

We, therefore, adopt it as the baseline model to gauge the impact of cooling.

While our simple isothermal model predicts *global* properties that are very similar to those seen in non-radiative simulations, it is clear that there are some differences between the two in terms of predicted *structural* properties. For example, Lewis et al. (2000) and, more recently, Loken et al. (2002) find non-isothermal temperature profiles in their non-radiative (“adiabatic”) simulations, with the gas temperature dropping by more than a factor of 2 from the cluster center to its periphery. Thus, it is reasonable to ask whether or not the isothermal model represents a fair baseline model. In order to test this, we turn to the study of Voit et al. (2003). Using the numerical simulations of Bryan & Voit (2001) (which were run with the same adaptive mesh refinement (AMR) code used by Loken et al. 2002), Voit et al. (2003) showed that the dimensionless entropy profiles of simulated non-radiative clusters are approximately self-similar. We use their self-similar entropy profile, which was kindly provided in electronic form by G. M. Voit and G. L. Bryan, together with a realistic dark matter density profile (the same profile used in the isothermal model) to construct a second baseline model to which we can compare our isothermal model. As expected, the global properties of the isothermal model and the non-radiative Voit & Bryan clusters are quite similar but there are some differences between the predicted temperature and density profiles. However, when we allow both baseline models to cool, we find very similar results (over a large range of masses), in the sense that both give rise to extremely high cooled gas fractions and both predict  $L-T$  relations which are too luminous (at a fixed temperature) with respect to the observations (we demonstrate this explicitly in §3 and §4 for the isothermal model). *Therefore, we find that including the effects of radiative cooling but not those of entropy injection leads to failure in accounting for observed properties of clusters. This conclusion holds irrespective of which baseline model we use.* Throughout the paper, we present results for the isothermal plus cooling model only.

Perhaps a more physically plausible model is one which includes both the effects of radiative cooling and entropy injection (e.g., Voit et al. 2002, 2003; Oh & Benson 2003). In order to examine this scenario, we will cool the entropy injection model of Babul et al. (2002). Like the isothermal model, the entropy injection model also consists of intracluster gas in hydrostatic equilibrium within a realistic dark halo. The primary difference between this model and the isothermal model (aside from the fact that one model assumes isothermality and the other does not) is that in the absence of cooling, the entropy injection model contains an isentropic core, which is presumed to have arisen through early heating events such as AGN outflows (e.g., Valageas & Silk 1999; Babul et al. 2002; Scannapieco & Oh 2004). The value of the entropy of this core is a free parameter and has been determined previously by fitting to observed scaling relations. Analysis of “cooling flow corrected” scaling relations, such as the  $L-T$  relation (Babul et al. 2002),  $M_{\text{gas}}-T$  relation (McCarthy et al. 2002a), and various SZ effect scaling relations (McCarthy et al. 2003b), indicates that an entropy core of  $\gtrsim 300 \text{ keV cm}^2$  gives the best fit. It is interesting to see whether or not such a high level of

injection is required once the effects of radiative cooling are also included and the results compared to actual uncorrected X-ray data. Before moving on, it is also worth noting that the entropy profile at large radii (where entropy injection is unimportant) in this model is not identical to that of our baseline isothermal model. Instead, the profile at large radii is required to match the results of high resolution non-radiative simulations (Lewis et al. 2000). We verify that the slope and normalization of the entropy profile at large radii is also a close match to the self-similar entropy profile reported by Voit et al. (2003).

## 2.2. A treatment of radiative cooling

Voit et al. (2002) clearly demonstrated that how one chooses to model the effects of radiative cooling can have a significant impact on the predicted properties of clusters (compare the results of their ‘truncated’ cooling model with their more realistic ‘radiative losses’ cooling model, for example). Thus, we wish to treat the effects of radiative cooling as realistically as possible but without resorting to computationally expensive hydrodynamic simulations. The treatment developed below is similar to the physically-motivated analytic method of Oh & Benson (2003) and the reader is referred to that study for a more in-depth discussion of boundary conditions and how the relevant differential equations are solved. We give a description of this method below.

We start with the initial gas and dark matter radial profiles for the model clusters (i.e., the profiles predicted by the isothermal and entropy injection models described above) and subject these to radiative cooling. Radiative cooling reduces the specific entropy ( $s$ ) of a parcel of gas according to

$$\frac{ds}{dt} = -\frac{\mu m_H n_i n_e \Lambda(T)}{\rho k_B T} \quad (1)$$

where  $\Lambda(T)$  is the cooling function (which is modeled as a Raymond-Smith plasma with 0.3 solar metallicity),  $\mu$  is the mean molecular weight (0.6 in this case), and the other symbols have their usual meanings.

Equation (1) can be re-written in terms of the gas pressure ( $P$ ) and the more commonly used form of ‘entropy’  $K$ , where  $s = \ln K^{3/2} + \text{constant}$  (assuming an ideal gas and an equation of state  $P = K\rho^{5/3}$ ),

$$\frac{dK}{dt} = -\frac{2}{3} \left( \frac{n_e n_i}{n^2} \right) \frac{1}{(\mu m_H)^2} \left( \frac{P}{K} \right)^{1/5} \Lambda(K, P) \quad (2)$$

The new gas entropy profile after cooling for a small time interval  $dt$  is calculated by integrating equation (2). The gas pressure is assumed to remain constant (i.e., isobaric cooling) over this short interval. After each time step, the properties of the gas (density and temperature and, therefore, pressure) are updated by placing the model clusters back in hydrostatic equilibrium by simultaneously solving the coupled differential equations

$$\begin{aligned} \frac{dr}{dM_{\text{gas}}} &= \frac{1}{4\pi r^2} \left( \frac{K}{P} \right)^{3/5} \\ \frac{dP}{dM_{\text{gas}}} &= -\frac{GM_{\text{DM}}}{4\pi r^4} \end{aligned} \quad (3)$$

As the gas cools and the pressure at the cluster center preferentially decreases, an inward flow develops in order to re-establish hydrostatic equilibrium. Because the gas flows inward, we must implement different boundary conditions than employed in setting up the initial cluster profiles (i.e.,  $M_{\text{gas,tot}}/M_{\text{tot}} = \Omega_b/\Omega_m$  at  $r_{\text{halo}}$ ). We solve for hydrostatic equilibrium after each cooling time step by applying the following boundary conditions (see Oh & Benson 2003):

$$\begin{aligned} r(0) &= 0 \\ r(M_{\text{gas,tot}}) &= r_{\text{end}} \\ P(M_{\text{gas,tot}}) &= \left[ P_{\text{halo}}^{2/5} + \frac{2}{5K_{\text{halo}}^{3/5}} \int_{r_{\text{end}}}^{r_{\text{halo}}} \frac{GM_{\text{DM}}(r)}{r^2} dr \right]^{5/2} \end{aligned} \quad (4)$$

where  $P_{\text{halo}}$  and  $K_{\text{halo}}$  are the initial gas pressure and entropy at  $r_{\text{halo}}$ , the maximum radius of cluster (see Babul et al. 2002 for a quantitative definition of  $r_{\text{halo}}$ ). The last boundary condition implies that the outermost gas mass shell is compressed adiabatically as it flows inward, which is appropriate since the cooling time of this shell greatly exceeds the age of the cluster. Since this is a two point boundary value problem (with  $r_{\text{end}}$  being the eigenvalue of the problem), we use a relaxation technique to solve the equations.

If cooled long enough, the temperature of the gas at the center of the model clusters will approach zero and cease to emit X-rays. This is referred to as ‘dropping out’. For the purposes of the present model, we assume a parcel of gas drops out (and is then removed from the calculation) if its temperature falls below  $\approx 10^5$  K or if its entropy decreases to zero during a time step. As the gas at the cluster center approaches this threshold, the time steps are chosen such that only a few mass shells drop out at a time. Typically, this corresponds to a temporal resolution of 20 Myr (depending on system mass), which is small compared to the age of the cluster and is more than sufficient to achieve convergent results. As the gas starts to drop out, a cooling flow is established. This flow is treated as an adiabatic process after the small time step  $dt$  by shifting the remaining (hot) gas,  $K(M_{\text{gas}})$ , inward to replace the mass shells that dropped out. The properties of the gas are then updated via hydrostatic equilibrium (as described above) and the cluster continues to cool. Similar to Oh & Benson (2003), we do not consider the effects of the cold gas on the gravitational potential of the cluster (e.g., adiabatic contraction of the dark matter halo). However, we do not expect this to significantly modify our results as our entropy injection + cooling model generally predicts small cooled gas fractions (which are consistent with observations).

An obvious but important question is how long should cooling be allowed to operate? For the sake of simplicity, it has become standard to allow the model clusters to cool for a Hubble time,  $t_h$  (e.g., Bryan 2000; Voit & Bryan 2001; Voit et al. 2002; Xue & Wu 2002; Oh & Benson 2003). Clearly, this represents the maximum amount of cooling a cluster can undergo. We show later (in §4) that if one focuses solely on explaining relaxed CF clusters, that in fact a wide distribution of times (in addition to an entropy injection level of  $\lesssim 300$  keV cm<sup>2</sup>) is required in order to account for the scatter in the  $L - T$  and  $L - M$  relations. The possibility of a connection

between the intrinsic scatter in the  $L - T$  relation and variations in the time available for cooling was previously suggested by Scharf & Mushotzky (1997). Throughout the paper, we plot results that span cooling from  $t = 0$  to  $t = t_h$ .

### 3. THE EFFECTS OF RADIATIVE COOLING

We examine here the general effects of radiative cooling on the global and structural properties of isothermal and entropy injection model clusters. This will aid the discussions in §4 and §5 of comparisons with the observations.

#### 3.1. Cooled gas fractions

As discussed earlier, if a cluster is allowed to cool for a long enough time, eventually gas will drop out of the ionized X-ray emitting phase, become neutral, and possibly form stars. Since there are fairly good observational constraints on the fraction of a cluster’s baryons that are in the form of neutral gas (e.g., Donahue et al. 2000; Edge 2001; Edge et al. 2002) and stars (e.g., Cole et al. 2001; Lin, Mohr, & Stanford 2003), a key prediction of the theoretical models is the fraction of gas that completely cools out.

Plotted in Figure 1 is the percentage of gas that completely cools out as a function of cluster mass, entropy injection level, and time (as the clusters cool). The various line types demonstrate how the cooled fraction evolves as a function of time, while the different panels show how entropy injection affects the amount of gas that is able to completely cool. The level of injection is characterized by  $S$  (what X-ray observers often call the “entropy”), which is related to the  $K$  via

$$S \equiv \frac{k_b T}{n_e^{2/3}} = K \left( \frac{n}{n_e} \right)^{2/3} (\mu m_H)^{5/3} \quad (5)$$

Concentrating for a moment on the upper left hand panel of Fig. 1, it can be seen that given nearly a Hubble time to cool, low mass clusters that have not been injected with entropy can cool out a substantial fraction ( $\gtrsim 20\%$ ) of their baryons. Yet, observations indicate that, at most, only 10% of a cluster’s baryons are in the form of stars (see Balogh et al. 2001). A negligible amount is in the form of neutral gas (see Edge et al. 2002). Simply reducing the amount of time that such systems can cool for (within reason) does not resolve this problem (see the dotted line, for example). This predicted overabundance of cooled material in groups and clusters has been dubbed the “cooling crisis” and has been taken as strong evidence in support of feedback/entropy injection (Balogh et al. 2001; Oh & Benson 2003). The requirement for large amounts of feedback/entropy injection also seems to be necessary in order to quench a similar problem found in semi-analytic and hydrodynamic studies of galaxy formation (Somerville & Primack 1999; Yoshida et al. 2002; Benson et al. 2003).

Encouragingly, the results for the isothermal plus cooling model are quite similar to those found from other analytic cluster models that include the effects of radiative cooling but not entropy injection (e.g., Voit et al. 2002; Oh & Benson 2003). This is despite there being slight differences in the adopted initial cluster conditions and

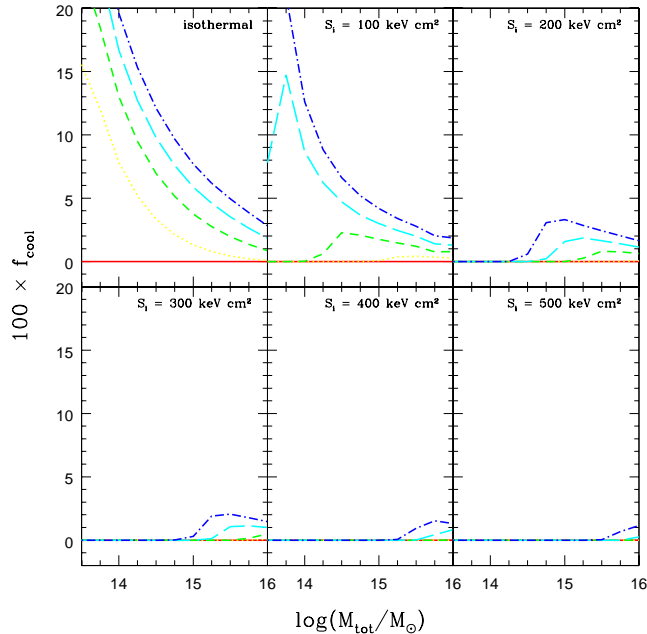


Fig. 1. Percentage of the total gas mass that completely cools out as a function of total cluster mass, time, and entropy injection level  $S_i$ . The cooled gas fraction,  $f_{\text{cool}}$ , is given by  $M_{\text{cool}}/(M_{\text{cool}} + M_{\text{hot}})$ , where  $M_{\text{cool}}$  is the total mass of gas that has cooled out of the X-ray emitting phase and  $M_{\text{hot}}$  is the total mass of gas remaining in the hot ionized phase. The solid, dotted, short dashed, long dashed, and dot dashed lines represent cooling for 0, 3, 6, 9, and 12 Gyrs, respectively. The different panels indicate how various levels of entropy injection affect the amount of gas that is able to completely cool out.

how one chooses to model the effects of cooling. This model also predicts cooled gas fractions which are comparable, although slightly lower, than those found from numerical simulations that include radiative cooling only (e.g., Muanwong et al. 2002; Davé, Katz, & Weinberg 2000).

Examination of the remaining panels in Fig. 1 clearly demonstrates that entropy injection has a large effect on the amount of gas that is able to cool out of the X-ray emitting phase. In particular, injecting the gas with  $S_i \gtrsim 200 \text{ keV cm}^2$  is sufficient to obtain cooled gas fractions consistent with the observations, while injecting more than  $300 \text{ keV cm}^2$  essentially shuts off cooling in all but the most massive clusters. Hence, entropy injection offers a viable solution to the so-called cooling crisis (see Oh & Benson 2003 for a detailed discussion).

### 3.2. Entropy profiles

Through hydrostatic equilibrium, the properties of the hot X-ray emitting gas at any particular time are determined entirely by the entropy distribution of the gas and the structure of the cluster's dark matter halo (see eqns. 3 and 4). Since radiative cooling modifies the cluster's entropy profile (see eqn. 2) it must also effect the cluster's gas density and temperature. These, of course, set the cluster's appearance and dictate how efficiently the cluster can continue cooling. Understanding how cooling modifies the entropy distribution of a cluster, therefore, is of paramount importance in understanding how it influences the evolution of a cluster's global and structural

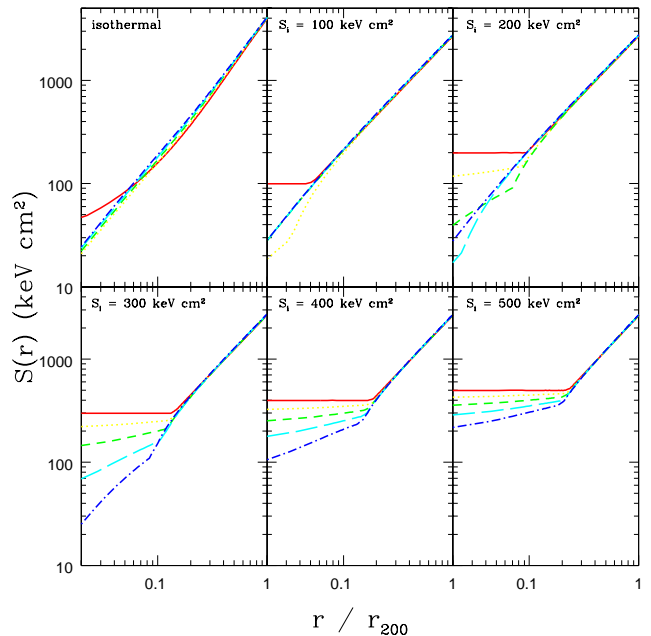


Fig. 2. The entropy profile as a function of time and entropy injection level for a cluster with  $M_{\text{tot}} = 10^{15} M_{\odot}$ . The line types have the same meaning as in Fig. 1. The quantity  $r_{200}$  is defined as the radius within which the mean dark matter density is 200 times the critical density of the universe (1.68 Mpc in this case).

properties.

Figure 2 shows the evolution of the entropy profile of a cluster with  $M_{\text{tot}} = 10^{15} M_{\odot}$  as a function of time. The various panels demonstrate how varying levels of entropy injection influence this evolution.

Let us focus first on the upper right hand panel of Fig. 2, since it shows the full range of entropy profiles as a function time. The initial entropy profile (solid line) shows a central floor of  $200 \text{ keV cm}^2$  (by design) and a power law of  $S \propto r^{-1.1}$  at large radii, which matches the large radii results of semi-analytic smooth accretion models and high resolution non-radiative simulations (Lewis et al. 2000; Tozzi & Norman 2001; Voit et al. 2003). After approximately 3 Gyr of radiative cooling, the central entropy of the cluster has dropped to nearly  $100 \text{ keV cm}^2$ . At this point, a clear entropy floor persists. As the cluster continues to cool, the entropy core steepens until eventually the central entropy approaches zero. When this occurs, gas begins to drop out of the X-ray emitting phase and an inward cooling flow develops. However, even after 9 Gyr of cooling a remnant of the initial entropy is still present (note the kink in the entropy profile near  $0.03 r_{200}$ ), although the 'core' is now quite steep and very small in radial extent (since most of it has dropped out). Eventually, the entropy core completely drops out and what remains is essentially a pure power law,  $S \propto r^{-1.1}$ , that extends all the way from the cluster center to its periphery. After this, the cluster continues to cool but approximately maintains this power law over all radii, reaching a quasi-steady state<sup>7</sup>.

<sup>7</sup> We use the phrase *quasi-steady state* instead of just steady state since, although the entropy profile maintains the same shape and normalization, it continues to decrease in radial extent with time as the gas flows inward to re-establish hydrostatic equilibrium.

The remaining panels in Fig. 2 are now easily interpreted. Our baseline isothermal model, which has the lowest initial central entropy, starts cooling gas out the fastest and it is simple to see why this model predicts such large cooled gas fractions (Fig. 1). Injecting the gas with  $100 \text{ keV cm}^2$  only slightly delays the development of a cooling flow. Injection levels of  $S_i = 300 \text{ keV cm}^2$  or higher, however, essentially prevent any gas from dropping out, although the central entropy of the gas is significantly lower after cooling for a Hubble time.

The above trends hold true for clusters with masses different than that considered in Fig 2. as well. The only difference is the amount of time it takes for the entropy profile to evolve. For example, because low mass clusters have lower central densities than high mass clusters (and, therefore, are less luminous), they have a much more difficult time in cooling out their entropy cores. On the other hand, clusters more massive than the one considered in Fig. 2 cool out their cores more quickly and reach the quasi-steady state faster.

The fact that radiative cooling approximately maintains the initial power-law entropy profile with time is interesting and deserves some investigation. First, it is worth noting that both the isothermal and entropy injection models approximately maintain their power-laws (once the elevated entropy at the center cools out). This is despite the fact that the power-law indices are not identical for these two cases. In particular, at large radii, the entropy injection model initially has  $S \propto r^{1.1}$  while the isothermal model initially has  $S \propto \rho^{-2/3} \propto r^{4/3}$  ( $\rho \propto r^{-2}$  at large radii for this model). Therefore, the fact that the power-law remains essentially invariant with cooling appears to be independent of the power-law index. We have verified that this is roughly true for a range of different initial power-law indices. Interestingly, a very similar trend has recently been reported by Kaiser & Binney (2003). These authors demonstrated that radiative cooling does not significantly modify the initial power-law relationship between entropy and gas mass of their model clusters. Unfortunately, a straightforward analytic explanation for these (numerically-derived) trends is not easily obtained, at least at small radii. At large radii, however, we should expect the power-law to be maintained since the cooling time of the gas is long relative to the Hubble time. This implies that  $S(M_{\text{gas}})$  should remain roughly constant and, furthermore, the physical size of a mass shell should be fixed (since the shell will not have been compressed much). Understanding the evolution of the entropy profile at small radii is more difficult because both coordinates,  $S(M_{\text{gas}})$  and  $r(M_{\text{gas}})$ , are being significantly modified by cooling. A more thorough investigation of entropy evolution of clusters will be presented in a forthcoming paper.

Given enough time, our models predict that all clusters should reach a quasi-steady state that is characterized by a near perfect power law entropy profile over all radii. However, since the age of the universe (which is an upper limit on the amount time available for cooling) is comparable to the predicted central cooling times of our model clusters, a general prediction of our model is that there should be a full range of central entropy distributions, depending on the initial injection level and how long each cluster is able to cool. Indeed, in §5 we demonstrate that

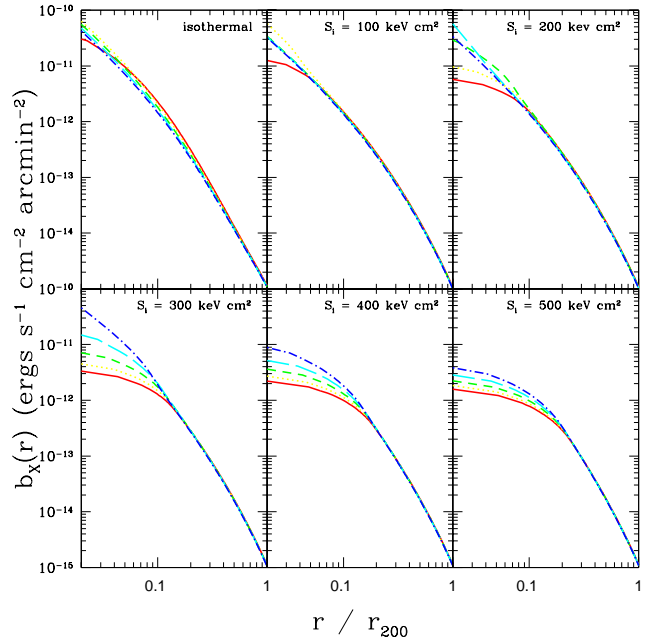


Fig. 3. The bolometric X-ray surface brightness profile as a function of time and entropy injection level for a cluster with  $M_{\text{tot}} = 10^{15} M_{\odot}$ . The line types have the same meaning as in Fig. 1.

new published *Chandra* and *XMM-Newton* results show a large range of central entropies that compares quite favorably to those plotted in Fig. 2.

### 3.3. Surface brightness and emission-weighted temperature profiles

Plotted in Figure 3 is the evolution of the bolometric X-ray surface brightness ( $b_X$ ) profile of a cluster with  $M_{\text{tot}} = 10^{15} M_{\odot}$  as a function of time. The panels and line types have the same meaning as in Figs. 1 & 2.

Again, we focus first on the model with an injection level of  $S_i = 200 \text{ keV cm}^2$  (upper right hand panel). It can clearly be seen that as the cluster cools the surface brightness near the center of cluster increases and becomes more peaked. This, of course, is due to the increasing central density which, in turn, is the result of the decreasing central entropy and the re-adjustment of the cluster gas to achieve hydrostatic equilibrium. Thus, there is a strong connection between the evolution of the surface brightness profile and the evolution of the entropy profile of a cluster. Indeed, comparison of Fig. 3 with Fig. 2 demonstrates that the central surface brightness is a strong function of the amount of low entropy gas near the cluster center. For example, the central surface brightness reaches its maximum value after roughly 9 Gyr of cooling (long dashed line), which coincides exactly with the time when the central entropy reaches its lowest value (i.e., just before the core drops out). Once the entropy core disappears, the surface brightness profile achieves a quasi-steady state (dot dashed line). This is expected given the results of §3.2. The same is true for other levels of entropy injection, the only difference being the time it takes to achieve this quasi-steady state (which are greater than a Hubble time for sufficiently high levels of entropy injection).

The trend of increasing central concentration of  $b_X$  as



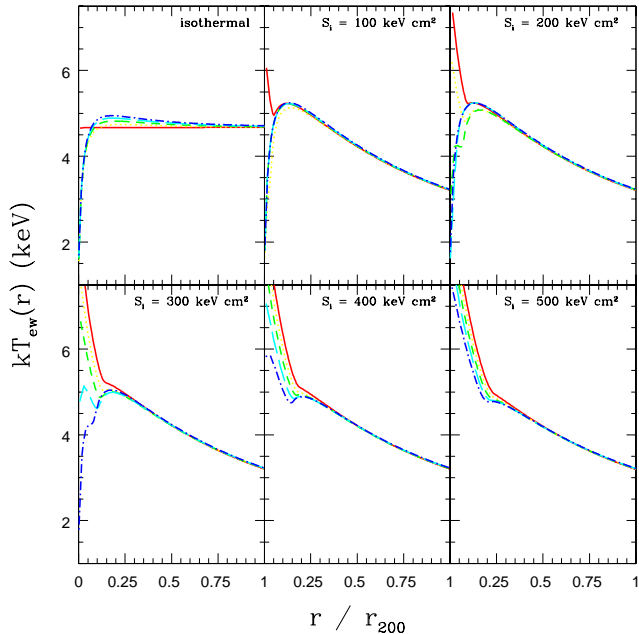


Fig. 4. The emission-weighted temperature profile as a function of time and entropy injection level for a cluster with  $M_{\text{tot}} = 10^{15} M_{\odot}$ . The line types have the same meaning as in Fig. 1.

the cluster cools is an interesting one. For clusters that had a mild level of entropy injection (top three panels of Fig. 3), radiative cooling has a large effect on the central gradient of the cluster’s surface brightness. On the other hand, clusters that had a large injection of entropy are less affected by cooling, as expected. This difference in central concentration means we can qualitatively identify the two types of clusters (i.e. those with mild and strong heating) with CF and NCF clusters, respectively (see §5.2). In fact, we argue later, on the basis of the observed  $L-T$  and  $L-M$  relations, that the origin of these two morphological classes of clusters can be explained in terms of the entropy injection level. This hypothesis is reinforced by the actual observed entropy profiles of these two classes of systems, which is presented in §5.

In Figure 4 we plot the evolution of the bolometric emission-weighted temperature ( $kT_{\text{ew}}$ ) profile of a cluster with  $M_{\text{tot}} = 10^{15} M_{\odot}$  as a function time. Again, the panels and line types have the same meaning as in the previous figures.

In the top three panels of Fig. 4, we see the rapid development of large positive temperature gradients at the cluster center. Like the surface brightness and entropy profiles discussed above, the emission-weighted temperature profile also reaches a quasi-steady state once the initial entropy core has dropped out. The predicted steady state temperature profile, which is characterized by a steep positive gradient at the cluster center and a gentle negative gradient at large radii, is qualitatively similar to that recently observed in CF clusters by Allen, Schmidt, & Fabian (2001) and De Grandi & Molendi (2002). On the other hand, clusters that had a high level of entropy injection ( $S_i > 300 \text{ keV cm}^2$ ) retain their sharp central negative temperature gradients even after cooling for more than 12 Gyr.

Lastly, it is also worth noting that the development of central positive temperature gradients in our models co-

incides almost exactly with the development of peaked surface brightness profiles. In other words, depending on the time elapsed since the entropy injection, one either has a cluster with a flat central surface brightness and a sharp central negative temperature gradient or a cluster with a peaked surface brightness profile and a central positive temperature gradient. These two types of clusters, which emerge naturally from our analytic model, match the main qualitative features of observed relaxed NCF and CF clusters.

### 3.4. Integrated luminosities and mean cluster temperatures

Figures 3 and 4 illustrate how radiative cooling is expected to modify the observable radial properties of the intracluster medium. Here, we describe the effects of cooling on the integrated X-ray luminosity and the mean emission-weighted temperature of the cluster.

As is evident from Figs. 2-4, cooling primarily affects only the central regions of the model clusters. Therefore, since cooling increases the central surface brightness and decreases the central temperature, we should expect that, in general, the integrated luminosity of the clusters will increase with the addition of radiative cooling while the mean temperature should decrease. This is exactly what the model predicts, as shown by the evolutionary  $L-T$  tracks plotted in Fig. 5. Here, the tracks of six clusters of varying mass are shown (dashed and dotted lines, see figure caption). The clusters evolve from the initial  $L-T$  relation predicted by the  $S_i = 200 \text{ keV cm}^2$  model without cooling (thick solid line) to higher luminosities. The open pentagons represent specific times of 0, 3, 6, 9, and 12 Gyr during the evolution.

To understand what this plot is telling us, let us focus for a moment on the tracks for the least massive (track A) and second most massive (track E) clusters. Track A shows that the least massive cluster starts off with a luminosity of  $L_{\text{X,bol}} \approx 6 \times 10^{43} \text{ ergs s}^{-1}$  and evolves to higher luminosities. After approximately 13 Gyr of cooling (i.e., the end of the track), the cluster’s luminosity has increased by roughly a factor of 3.3. Also, its temperature has decreased but not by nearly as much (only a factor of 1.19). Thus, the evolution in the  $L-T$  plane is primarily driven by the influence of cooling on the luminosity rather than the temperature. It is important to note that even after 13 Gyr of cooling this low mass cluster has been unable to rid itself of its initial entropy core (see Fig. 1). Therefore, it is straightforward to understand why the  $L-T$  relation evolves as it does: with time the central entropy decreases, giving rise to an increased central density which, in turn, dramatically increases the X-ray luminosity of the cluster. More massive clusters experience something slightly different. Focusing on track E, we see that just shortly after 6 Gyr of cooling the cluster begins to evolve back towards lower luminosities and higher temperatures (as indicated by the dotted line). Eventually, after approximately 9 Gyr, it reaches a more or less stable position on the  $L-T$  diagram. These trends can be understood by re-examining the results presented in §3.3. First, the fact that the cluster reaches a stable position on the  $L-T$  diagram is expected since it has been shown that the surface brightness and temperature profiles reach quasi-steady states.

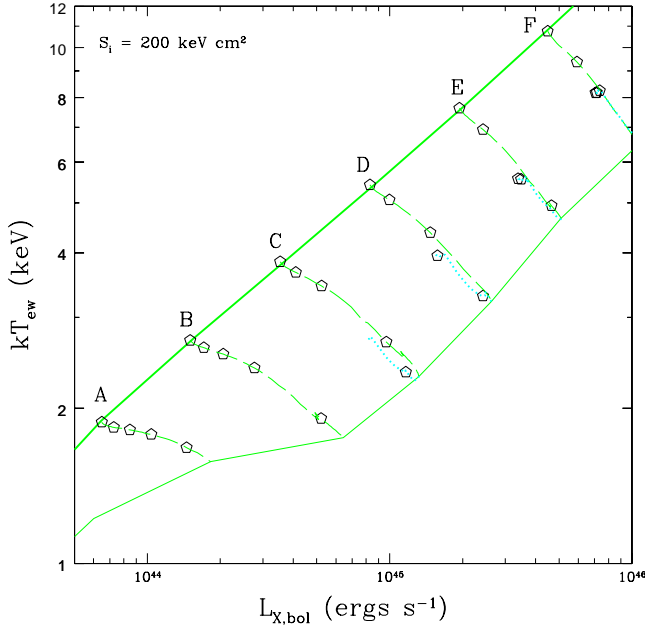


Fig. 5. Evolutionary  $L - T$  tracks for clusters that have been injected with  $S_i = 200 \text{ keV cm}^2$ . Six different tracks are shown corresponding to clusters with masses of  $\log_{10}(M_{\text{tot}}) = 14.25$  (A), 14.50 (B), 14.75 (C), 15.00 (D), 15.25 (E), and 15.50 (F) (in  $M_\odot$ ). The thick solid line is the initial  $L - T$  relation prior to including the effects of radiative cooling. The dashed and dotted lines are the evolutionary tracks as the cluster cools. The dashed lines show evolution towards high  $L$  and low  $T$ , which occurs prior to the removal of the isentropic core, while the dotted lines show the evolution towards low  $L$  and high  $T$ , which occurs after the core has dropped out (if it is able to drop out in less than 13 Gyr). Together, the thin and thick solid lines enclose the predicted range of  $L - T$  values during cooling for 13 Gyr. For comparison with the previous figures, the open pentagons show the predicted  $L - T$  relation at the discrete times of 0, 3, 6, 9, and 12 Gyr.

Given the results of §3.3, it is also clear why this stable point happens to lie at a higher luminosity/lower temperature than the initial  $L - T$  relation (i.e., the surface brightness is more peaked while the temperature profile shows a central positive gradient). Furthermore, we can also understand the origin of the turn-around of this massive cluster on the  $L - T$  diagram as being due to the entropy core in its final days. Just prior to the dropping out of the entropy core, there exists a large amount of low entropy gas near the cluster center (since the core cools somewhat intact, see top right hand panel of Fig. 2). This gives rise to an extremely peaked surface brightness profile. However, once the core completely drops out, the surface brightness peak is diminished (so, too, is the integrated luminosity) and, hence, the result is the  $L - T$  turn-around.

As might be expected, the above trends also hold true for clusters that have experienced different levels of entropy injection. Even clusters that were initially isothermal (and have no core per se) evolve towards higher luminosities and lower temperatures. This seems to be a very general prediction of our cooling model for massive clusters. Encouragingly, Voit et al.'s (2002) ‘radiative losses’ model, which is similar to our model in many aspects, also predicts an overall evolution of the  $L - T$  relation

towards higher luminosities and lower temperatures and by roughly the same magnitude (see their Fig. 27).

Figure 5 shows that the position of any given cluster on the  $L - T$  diagram is dictated by the initial level of entropy injection and how long radiative cooling has had to operate. (See also Figure 9 for predicted  $L - T$  relation for a range of entropy injection levels.) This implies a potential degeneracy in the sense that one can account for the observed location of any individual cluster on the  $L - T$  diagram as being due to either a high level of initial entropy injection and a long subsequent period of cooling, or a low level of initial entropy injection followed by a relatively short period of cooling. However, this degeneracy is bounded. There are regions of the  $L - T$  plot (see Figure 9) that cannot be accessed by clusters with  $K_0 > 300 \text{ keV cm}^2$ , even if they cooled for the entire lifetime of the Universe. Similarly, there are regions of the  $L - T$  plot that cannot be accessed by clusters with low initial entropy injection. Jointly, these two bounds can be used to place rough constraints on the initial entropy injection of an individual cluster. On the other hand, as we discuss below, the distributions of present-day global and structural properties of the cluster population, collectively, provide a powerful probe of the initial *distribution* of entropy injection levels. Additional insights are also likely to be obtained from an analysis of a high- $z$  cluster sample because radiative cooling will not have had much time to operate in these systems.

Before proceeding with a comparison of our models with the observational data, we stress that there is an important caveat to the results presented in this subsection. As noted earlier, if a cluster is able to cool out its initial entropy core, what remains is pure power law entropy profile with the cluster achieving a quasi-steady state. This gives rise to a more or less fixed position on the  $L - T$  diagram. This is only true, however, if the radial extent of the entropy profile is not reduced by a significant amount after a Hubble time of cooling. Under the circumstances considered above, i.e., high mass clusters and fairly large amounts of entropy injection, this condition is approximately met. Because such clusters are only able to cool out a small fraction of their baryons, gas that was originally at the outskirts of the cluster only manages to flow inward by a relatively small amount. However, in the limit of low mass clusters that experience small amounts of entropy injection (and, therefore, extremely high cooled gas fractions), the shrinking entropy profile can significantly affect the evolution of the  $L - T$  relation. The amount of gas that remains in the hot X-ray emitting phase after a Hubble time of cooling is reduced by a large fraction and so, too, is the X-ray luminosity of the cluster. The result is a position on the  $L - T$  diagram that is actually at a lower luminosity and higher temperature than the initial position (i.e., to the left of the initial curve). In fact, the same would be true of high mass clusters if they could somehow be forced to cool out  $\gtrsim 15 - 20\%$  of their baryons. We have tested this by allowing our high mass clusters to continue cooling for several Hubble times until they reach this cooled gas fraction. Thus, the resulting  $L - T$  relation is a strong function of the efficiency of cooling in clusters. It is, therefore, essential that the model retain consistency with the observed cooled gas fraction of clusters.



## 4. COMPARISON WITH OBSERVED GLOBAL PROPERTIES

The luminosity-temperature relation has been known for roughly a decade now to deviate from simple self-similar predictions. This has been the primary motivating factor for the investigation of cluster models that incorporate non-gravitational gas physics, such as entropy injection and/or radiative cooling. While such models have generally been shown to provide better matches to the ‘typical’ cluster, the large amount of intrinsic scatter in the observed  $L - T$  (e.g., Novicki, Sornig, & Henry 2002) and  $L - M$  (e.g., Reiprich & Böhringer 2002) relations has yet to be addressed by these models. A primary goal of the present study is to see whether or not the scatter is consistent with theoretical models that include entropy injection and/or radiative cooling.

## 4.1. Observations

Essential to exploring the properties of the scatter are large, homogeneously analysed samples of clusters. Such samples guard against selection effects, differences in analysis procedures, differences in absolute flux calibration between various instruments, and other issues which could influence the physical interpretation of the scatter. Ideally, these samples should not have had any corrections applied to them (e.g., “cooling flow” correction) other than the removal of obvious point sources (e.g., McCarthy, West, & Welch 2002b). Fortunately, such samples are now becoming available. We focus on two of the larger samples that now exist: the *ASCA* Cluster Catalog (ACC) of Horner (2001) and the extended *ROSAT* HIFLUGCS sample of Reiprich & Böhringer (2002).

The ACC of Horner (2001) contains roughly 270 clusters, the large majority of which are nearby systems ( $z \leq 0.2$ ) (and, henceforth, we restrict ourselves to nearby clusters with  $z \leq 0.2$ ). The wide bandpass and good spectral resolution of *ASCA* allows for the accurate determination of cluster mean temperatures and total bolometric X-ray luminosities. Unfortunately, because of *ASCA*’s rather poor spatial resolution, it is not possible to accurately measure surface brightness profiles and, therefore, quantities such as cluster mass. Thus, we use the ACC by itself to study the luminosity-temperature relation only. In order to study the luminosity-mass relation of clusters, we turn to the extended HIFLUGCS sample. Using surface brightness profiles from *ROSAT* and temperatures from *ASCA*, Reiprich & Böhringer (2002) deduced, through the assumption of hydrostatic equilibrium (and isothermality), the masses of 106 nearby ( $z \lesssim 0.2$ ) clusters within three different radii:  $r_{500}$ ,  $r_{200}$ , and a fixed physical radius of  $3h_{50}^{-1}$  Mpc. In the present study, we focus only on the mass within  $r_{500}$ , which is typically the smallest of the three and, therefore, requires the least amount of extrapolation of the observed surface brightnesses (see Reiprich & Böhringer 2002). Unfortunately, many of the temperatures used by these authors were corrected for the effects of “cooling flows” and, therefore, in its current state, the sample cannot be fairly compared to our radiative cooling models. In order to address this issue, we have selected clusters in common between the ACC and the HIFLUGCS ( $\approx 80$  systems). Using uncorrected temperatures from the ACC and surface brightness profiles from the HIFLUGCS, we recompute the cluster masses within

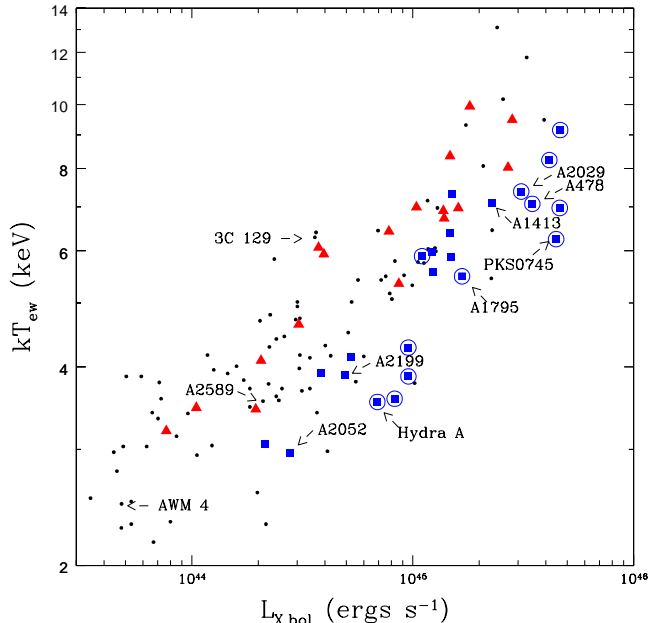


Fig. 6. The observed  $L - T$  relation of nearby, massive galaxy clusters. Data are from the *ASCA* Cluster Catalog of Horner (2001). Small filled circles represent clusters that have no published cooling flow status. Triangles represent clusters that have an inferred cooling flow mass deposition rate,  $\dot{M}$ , consistent with zero, squares represent clusters with  $\dot{M} \gtrsim 100 M_{\odot} \text{ yr}^{-1}$ , and squares with a surrounding open circle represent clusters with  $\dot{M} \gtrsim 300 M_{\odot} \text{ yr}^{-1}$ . Cooling flow deposition rates were estimated by Allen & Fabian (1998) and Peres et al. (1998) based on a deprojection analysis of *ROSAT* data. The clusters that have been labeled are those which now have published entropy profiles inferred from *Chandra* or *XMM-Newton* observations.

$r_{500}$ , taking care to correct for differences in the assumed cosmologies.

Before comparing the observed scaling relations to the models, it is instructive to examine the properties of the data itself. Plotted in Figure 6 is the observed luminosity-temperature relation of nearby, massive clusters. Where possible, we indicate with symbols the cooling flow status of the clusters. In particular, triangles represent clusters that have an inferred cooling flow mass deposition rate,  $\dot{M}$ , consistent with zero, squares represent clusters with  $\dot{M} \gtrsim 100 M_{\odot} \text{ yr}^{-1}$ , and squares with a surrounding open circle represent clusters with  $\dot{M} \gtrsim 300 M_{\odot} \text{ yr}^{-1}$ . Cooling flow deposition rates were estimated by Allen & Fabian (1998) and Peres et al. (1998) based on a deprojection analysis of *ROSAT* surface brightness data. Those clusters that have published deprojected entropy profiles (or deprojected temperature and density profiles from which an entropy profile may be derived) inferred from new *Chandra* or *XMM-Newton* data have been explicitly labeled and will be examined in detail in §5.

First, there is the expected well-defined correlation between a cluster’s luminosity and temperature. However, there is a large amount of scatter in the plot. As discussed by Allen & Fabian (1998), correcting for the central “cooling flow” dramatically reduces the scatter in the  $L - T$  relation. Here, we have purposely left the

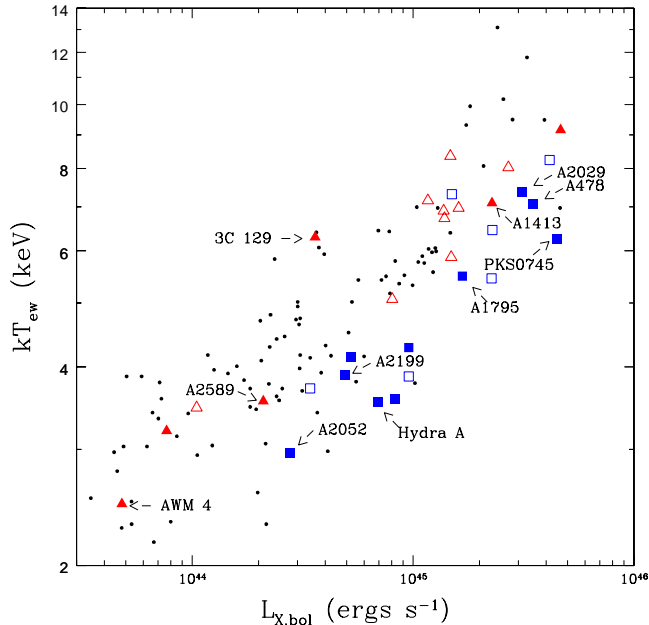


Fig. 7. Same as Fig. 6 but using published *Chandra* and *XMM-Newton* data to classify the clusters according to CF status and morphology. Here, squares represent CF clusters, triangles represent NCF clusters, filled symbols represent relaxed systems, and open symbols represent unrelaxed systems.

data uncorrected for the effects of “cooling flows” in an attempt to ascertain whether models that include radiative cooling (either alone or in addition to some amount of entropy injection) can account for this scatter.

There is also a high degree of coherent structure present in the scatter of the  $L - T$  relation. Namely, the clusters with large values of  $\dot{M}$  preferentially lie on the high luminosity side of the scaling relation, while clusters with small values of  $\dot{M}$  lie on the low luminosity side. This correlation between inferred cooling flow strength and dispersion in the scaling relation has been known for some time (Fabian et al. 1994; see also White, Jones & Forman 1997; Allen & Fabian 1998; Markevitch 1998). However, Fig. 6 is probably the cleanest, most clearcut illustration of this trend to date, with the high and low  $\dot{M}$  systems occupying well-defined loci.

Recently, the standard isobaric cooling flow model has been shown to provide a poor description of *XMM-Newton* spectra of CF clusters (e.g., Peterson et al. 2001, 2003; Kaastra et al. 2004). Thus, the inferred mass deposition rates may not be perfect indicators of whether a cluster is a “cooling flow” cluster or not (i.e., whether or not it contains a peaked surface brightness and a central positive temperature gradient). This is important if we wish to quantify comparisons between the models and CF or NCF clusters. In order to test this idea, we searched the literature for new *Chandra* and *XMM-Newton* observations of clusters in the Horner ACC and classified each system as either CF or NCF, and either relaxed or unrelaxed. Determination of CF versus NCF status is based primarily on the presence or absence of a well-defined central positive temperature gradient, while determination of the dynamical state is determined by the presence or absence of large-scale ( $\sim$  a few hundred

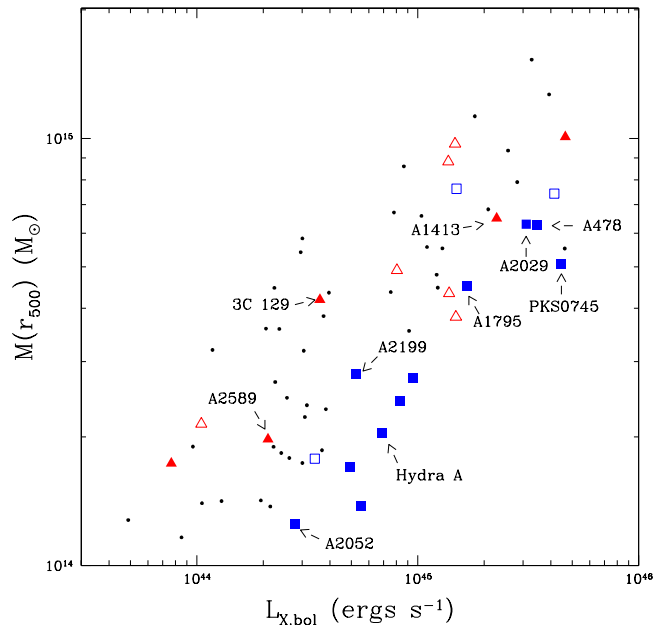


Fig. 8. The observed  $L - M$  relation of nearby, massive galaxy clusters. Luminosities are from Horner (2001) and masses are computed using the surface brightness profiles of Reiprich & Böhringer (2002) and uncorrected temperatures of Horner (2001). The symbols have the same meaning as in Fig. 7.

kpc) substructure in the X-ray images, which is presumably due to mergers. *Therefore, our classification scheme makes use of observed features rather than quantities inferred by fitting an assumed model.* The results of this classification are presented in Figure 7 for the  $L - T$  relation and Figure 8 for the  $L - M$  relation. Table 1 lists the clusters plotted in Figs. 7 and 8 along with their classifications.

An examination of Fig. 7 demonstrates that our “cooling flow” classification scheme correlates well with the results plotted in Fig. 6, although the results in Fig. 7 look less impressive since, to date, only a relatively small number of clusters in the ACC have been observed by *Chandra* or *XMM-Newton*. Furthermore, Fig. 7 indicates that there are apparently more unrelaxed NCF systems than relaxed systems. It is important to note, however, that the majority of NCF clusters observed with *Chandra* to date have been selected because they were known to be mergers (for the purposes of studying bow shocks, etc.). This is discussed further in §6 & 7. Interestingly, several of the clusters that lie roughly on the boundary between high and low  $\dot{M}$  systems in Fig. 6 have switched “cooling flow” classification in Fig. 7 (e.g., A1413, A1689). More importantly is that, *in general, the dynamical status of a cluster does not seem to influence its position on the  $L - T$  diagram* (note that the relaxed and unrelaxed NCF clusters lie together in one locus while relaxed and unrelaxed CF clusters lie together in another). This point is discussed further in §5 and 6.

The  $L - M$  relation plotted in Fig. 8 has many of the same features present in the  $L - T$  relation. Namely, NCFs and CFs are separated according to luminosity, and dynamical status does not seem to systematically affect this trend. As far as we are aware, this is the first

TABLE 1  
PROPERTIES OF NEARBY CLUSTERS BASED ON ANALYSIS OF CHANDRA/XMM-NEWTON DATA

Cluster	CF/NCF	relaxed?	references
2A 0335+096	CF	yes	Mazzotta et al. (2003)
3C 129	NCF	yes	Krawczynski (2002)
A85	NCF	no	Kempner et al. (2002)
A115	CF	no	Gutierrez & Krawczynski (2003)
A133	CF	no	Fujita et al. (2002)
A478	CF	yes	Sun et al. (2003a)
A496	CF	yes	Dupke & White (2003)
A644	CF	no	Lewis & Buote (2002); Bauer & Sarazin (2000)
A665	NCF	no	Markevitch & Vikhlinin (2001)
A1060	NCF	yes	Yamasaki et al. (2002)
A1068	CF	no	Wise et al. (2004)
A1367	NCF	no	Sun & Murray (2002)
A1413	NCF	yes	Pratt & Arnaud (2002)
A1689	NCF	yes	Xue & Wu (2002)
A1795	CF	yes	Ettori et al. (2002)
A2029	CF	yes	Lewis et al. (2003)
A2034	NCF	no	Kempner et al. (2003)
A2052	CF	yes	Blanton et al. (2003)
A2142	CF	no	Markevitch et al. (2000)
A2199	CF	yes	Johnstone et al. (2002)
A2218	NCF	no	Machacek et al. (2002)
A2256	NCF	no	Sun et al. (2002)
A2589	NCF	yes	Buote & Lewis (2004)
A2597	CF	yes	McNamara et al. (2001)
A3112	CF	yes	Takizawa et al. (2003)
A3266	NCF	no	Henriksen & Tittley (2002)
A3667	NCF	no	Mazzotta et al. (2002)
A3921	NCF	no	Sauvageot et al. (2001)
AWM4	NCF	yes	O'Sullivan & Vrtilek (2004)
Hydra A	CF	yes	David et al. (2001)
MKW4	CF	yes	O'Sullivan & Vrtilek (2004)
PKS 0745-19	CF	yes	Chen et al. (2003)
RX J1720.0+2638	CF	no	Mazzotta et al. (2001)

NOTE. — “Cooling flow” status is based on the presence or absence of large declining temperature profiles towards the cluster center while dynamical status is based on the presence or absence of large-scale irregularities (presumably due to merging) in the X-ray images of the clusters.

time the dispersion in the luminosity-mass relation has been shown to depend on “cooling flow” status, although Reiprich & Böhringer (2002) hinted at the existence of such a trend (ApJ, 567, pg. 730). Below, we examine whether any of the theoretical models can account for this intrinsic scatter and the dichotomy between NCF and CF clusters.

To begin with, we consider the issue of the cooling flow mass deposition rate,  $\dot{M}$ . The new *Chandra* and *XMM-Newton* high resolution X-ray data of massive CF clusters have been used to infer mass deposition rates typically ranging from  $\dot{M} \sim 100 - 400 M_{\odot} \text{ yr}^{-1}$  (e.g., Schmidt, Allen, & Fabian 2001; Ettori et al. 2002; Peterson et al. 2003), which is substantially lower than previous estimates based on *ASCA* and *ROSAT* data of the same clusters. Our model predicts mass drop out rates in range  $300 - 500 M_{\odot} \text{ yr}^{-1}$  once the initial entropy core has been radiated away. To the extent that these two results can be compared, we are comforted by the reasonable agreement. Admittedly, the model results appear to be somewhat larger than the “observed” values; however, we point out that the latter are inferred from the observations assuming an isobaric cooling flow model whereas our model values represent the actual physical cooling rate in the systems. Strictly speaking, a detailed comparison of the theoretical vs. “observed” mass drop out rates would entail making mock observations of our

model clusters and then, use the isobaric cooling flow model to infer a mass drop out rate for the theoretical models, an exercise that is beyond the scope of the present study.

#### 4.2. The $L - T$ relation

Plotted in Figure 9 is a comparison between the theoretical models and the observed  $L - T$  relation. The various panels show the predicted relation for a range of entropy injection levels. The thick solid lines in each panel represent the luminosity-temperature relation prior to including the effects of radiative cooling. The hatched regions encompass the full range of  $L - T$  values spanned by the model clusters during 13 Gyrs of cooling (similar to Fig. 5). The data is the same as that plotted in Fig. 7. We have not plotted error bars on the data as the statistical error bars on the luminosity are negligible and we have restricted ourselves to clusters with temperature determinations to better than 20% (i.e.,  $\Delta kT_{\text{ew}}/kT_{\text{ew}} \leq 0.2$ ). Thus, the intrinsic scatter in the relation dominates the statistical scatter.

The top left hand panel of Fig. 9 demonstrates why there has been so much effort invested in researching the role of non-gravitational gas physics in clusters. The thick solid line in this panel, which represents a model with no cooling and no entropy injection, clearly fails to match the observational data. It should be noted that

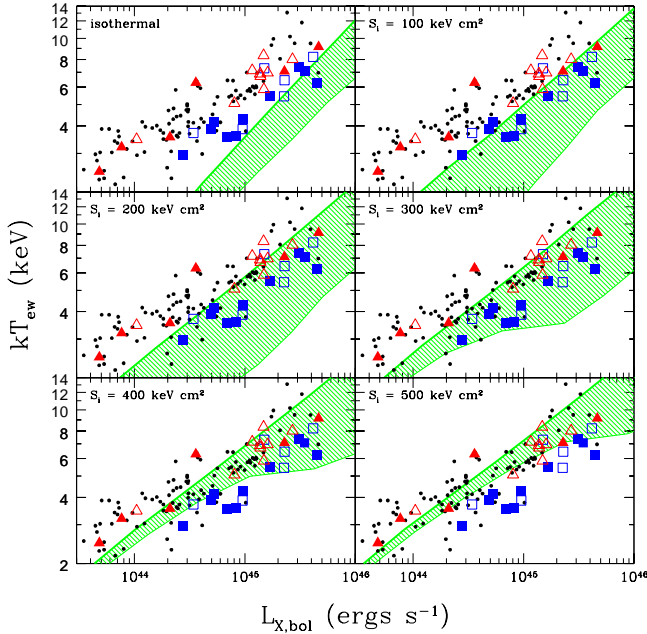


Fig. 9. Comparison of theoretical models to the observed  $L - T$  relation. The thick solid line represent the initial models prior to including the effects of cooling. The hatched region represents the full range of predicted  $L - T$  values during cooling for 13 Gyr. The symbols have the same meaning as in Fig. 7.

there is essentially no freedom in the isothermal model, unless one is willing to resort to a drastically different dark matter profile than the one currently being considered. Cooling the isothermal model over the course of 13 Gyr (hatched region) does not improve the situation. If anything, it makes things worse, as the clusters' luminosities increase with the inclusion of cooling. In addition, the model also violates the observed cooled gas fraction of clusters reported by Balogh et al. (2001) (see Fig. 1). As noted in §2.1, very similar results are obtained if, instead of using the isothermal model, we make use of the non-radiative self-similar entropy profile of Voit et al. (2003) to construct an alternative baseline model. This is compelling evidence that some form of entropy injection is required.

First we investigate models with only a single, fixed entropy injection level. For example, we have previously reported that an entropy injection level of  $> 300 \text{ keV cm}^2$  provides a good fit to the data (e.g., Babul et al. 2002; McCarthy et al. 2003b). The aim of these studies was to account for the properties of groups and clusters minus any “cooling flow” component and, therefore, the effects of radiative cooling were neglected by these models. A better approach (which we have adopted in the present study), however, is to include the effects of radiative cooling and explicitly try to model uncorrected data. Surveying the thick solid lines in each of the panels (i.e., entropy injection only models), it is seen that injecting the ICM with  $\approx 200 \text{ keV cm}^2$  gives the best fit to the *uncorrected* X-ray data (in the sense that the predicted relation falls more or less in the middle of the data). Injecting  $> 300 \text{ keV cm}^2$  tends to skew the predicted  $L - T$  relation towards lower luminosities (i.e., the region occupied by NCF clusters), confirming our previous results for fits to “cooling flow” corrected data. However, with

the large amount of intrinsic scatter present in the new uncorrected X-ray data, it is clear that no single entropy injection level can account for the uncorrected  $L - T$  relation.

Alternatively, we could consider a range of entropy injection levels. As with any physical process, a variation in efficiency is likely to be the norm. However, in order to explain systems on the high-luminosity side of the  $L - T$  relation (i.e., where CF clusters live), entropy injection levels of  $S_i \lesssim 300 \text{ keV cm}^2$  are required. The predicted central cooling time of massive clusters with this amount of injection is comparable to the Hubble time (see, e.g., Fig. 1) and, therefore, the effects of cooling need to be factored in. Additionally, as pointed out recently by Mushotzky et al. (2003), among others, simple entropy injection models cannot account for the observed entropy profiles of (some) groups and clusters, most likely because of the effects of radiative cooling. Central positive temperature gradients observed in many massive “cooling flow” clusters (e.g., Allen, Schmidt, & Fabian 2001) also attest to the importance of radiative cooling. In other words, the observations are unlikely to be explained by a model which includes a range of injection levels but not the effects of radiative cooling.

The alternative is to consider a model that includes both entropy injection and radiative cooling. Physically, this is probably the most plausible scenario anyway. However, as demonstrated by Fig. 9, it doesn't seem possible to explain all of the data with a single entropy injection level plus radiative cooling. An entropy injection level of  $S_i \approx 300 \text{ keV cm}^2$  probably comes the closest to explaining the data, but it is clear that a significant fraction of the clusters on the low luminosity side of the relation are not explained by this model. Increasing the injection level improves the situation but at the expense of losing agreement with the relaxed CF clusters. This makes sense since increasing the injection level mitigates the effects of radiative cooling. We are again forced to consider a model with a range of entropy injection levels but this time with the effects of radiative cooling included. With no constraints on the source of the entropy injection, indeed it can be seen from the trends in Fig. 9 that the data (including both relaxed CF and NCF clusters) can be accounted for by such a model. In particular, the CF clusters can typically be explained by entropy injection levels of  $S_i \lesssim 300 \text{ keV cm}^2$ , while NCF clusters require higher injection levels.

#### 4.3. The $L - M$ relation

While we place more weight on the  $L - T$  relation (because it is based on essentially WYSIWYG observables), it is still useful to examine the  $L - M$  relation as a consistency check. Figure 10 presents a comparison between the observed and predicted luminosity-mass relations<sup>8</sup>. Reassuringly, the same general trends may be derived from this plot as well; i.e., clusters on the low luminosity side of the relation can be explained by high levels of entropy injection, while clusters on the high luminosity side can be explained by low levels of entropy injection (plus radiative cooling). There are some slight differences, however, in the exact constraints placed on the injection levels by the  $L - T$  and  $L - M$  relations. These are probably due to issues associated with the analysis of the observational data as well as simplifying assumptions



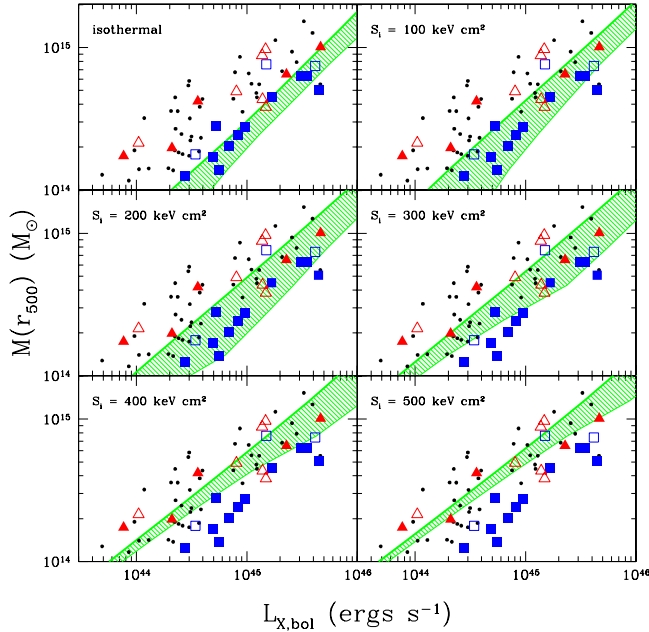


Fig. 10. Comparison of theoretical models to the observed  $L - M$  relation. The thick solid line represent the initial models prior to including the effects of cooling. The hatched region represents the full range of predicted  $L - M$  values during cooling for 13 Gyr. The symbols have the same meaning as in Fig. 7.

in the modeling [assumptions for the *observed mass* calculation include isothermality, an assumed form for the surface brightness profiles (i.e., beta model), and spherical symmetry].

#### 4.4. Summary

We have found that cooling only and entropy injection only models fail to reproduce the observed uncorrected luminosity-temperature and luminosity-mass relations of nearby massive clusters. However, a model that includes a distribution of entropy injection levels and radiative cooling can account for these relations, including their intrinsic scatter and the dichotomy between NCF and CF clusters. In particular, NCF and CF clusters require relatively large and small amounts of additional entropy, respectively, with  $S_i \approx 300 \text{ keV cm}^2$  essentially being the dividing line between the two classes of clusters. In retrospect, this result is not surprising, since the cooling threshold, assuming cooling for roughly a Hubble time, for a typical massive cluster with  $kT_{ew} \sim 6 \text{ keV}$  is  $\sim 300 \text{ keV cm}^2$  (see Fig. 1 of Voit & Bryan 2001).

Immediately below, we examine whether or not such a model can account for the observed structural properties of clusters, as deduced from new *Chandra* and *XMM-Newton* data.

<sup>8</sup> The observed values of  $M(r_{500})$  refer to the total mass (baryons and dark matter), whereas the model values neglect the baryon contribution. We have ignored the baryonic component in the models as hydrostatic equilibrium is computed using the dark matter potential only. However, this is a small effect that we can neglect since, at worst, the model masses are incorrect by a factor of  $\Omega_b/\Omega_m \approx 0.119$  while the measurements uncertainties are typically  $\sim 20\%$  (Reiprich & Böhringer 2002).

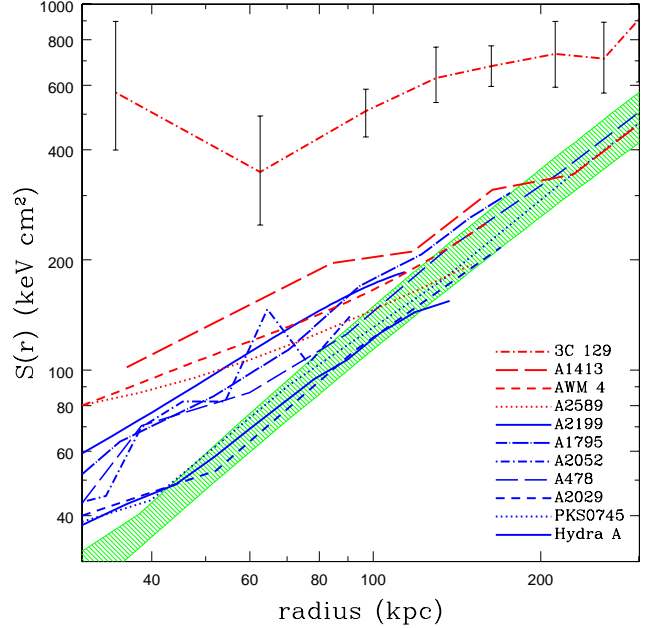


Fig. 11. The entropy profiles of 11 nearby, massive clusters observed with *Chandra* or *XMM-Newton*. The key in the bottom right hand corner is ordered according to the central entropy values of these clusters in descending order (i.e., 3C 129 is the top long dashed line, A1413 is the long dashed line immediately below, and so on). With the exception of 3C 129, errors on the derived entropy profiles are typically 10%. The hatched region represents the model predictions for clusters that are actively cooling gas out (see text).

## 5. COMPARISON WITH OBSERVED STRUCTURAL PROPERTIES

### 5.1. Entropy profiles

Presented in Figure 11 are the observed entropy profiles of the *relaxed* clusters labeled in Figs. 7 & 8 as derived from new *Chandra* and *XMM-Newton* data. These clusters include 3C 129 (Krawczynski 2002; *Chandra* data), A1413 (Pratt & Arnaud 2002; *XMM-Newton* data), AWM4 (O'Sullivan & Vrtillek 2003; *XMM-Newton* data), A2589 (Buote & Lewis 2004; *Chandra* data), A2199 (Johnstone et al. 2002; *Chandra* data), A1795 (Ettori et al. 2002; *Chandra* data), A2052 (Blanton et al. 2003; *Chandra* data), A478 (Sun et al. 2003a; *Chandra* data), A2029 (Lewis, Buote, & Stocke 2003; *Chandra* data), PKS0745 (Chen, Ikebe, & Böhringer 2003; *XMM-Newton* data) and Hydra A (David et al. 2001; *Chandra* data). In some cases, the actual deprojected entropy profile was not published but could be easily derived from the published deprojected temperature and density (or pressure) profiles. In such cases, we assume a  $0.3Z_\odot$  metallicity if none was listed. The hatched region is the predicted zone of entropy profiles from clusters with emission-weighted temperatures ranging from  $3 \text{ keV} \lesssim kT_{ew} \lesssim 9 \text{ keV}$  (roughly matching the observed range) and whose *initial entropy core has dropped out*. The value of the initial core is irrelevant since, once the core has dropped out, the resulting entropy profiles for clusters of a given mass are identical in the model of Babul et al. (2002). In other words, the hatched region illustrates where clusters that are actively cooling



gas out should live. If, however, the gas was injected with entropy and has not had enough time since to cool out the resulting entropy core, we should expect to see elevated entropy levels near the cluster center (see Fig. 2). At large radii, however, all of the profiles should converge to the hatched region, as this is the regime where shock heating becomes much more important than the non-gravitational entropy injection.

One of the first features that leaps out of Fig. 11 is that essentially all of the observed entropy profiles converge to the hatched region at large radii, where non-gravitational physics is less important. This suggests that high resolution numerical simulations are doing an excellent job of capturing the gravitational gas physics of cluster formation (again, we note that the entropy profile at large radii in our models has been forced to match the results of non-radiative simulations).

But how does the entropy injection plus cooling model measure up to the observed entropy profiles at small radii? The answer is surprisingly well. A comparison of Fig. 11 to Figs. 7 & 8 shows that there is a clear trend between central entropy and dispersion in the  $L - T$  and  $L - M$  relations. Namely, the central entropy increases as one goes from the high luminosity side to the low luminosity side of these relations. This is quite reminiscent of the trend between dispersion in the  $L - T$  and  $L - M$  relations and “cooling flow” status plotted in Figs. 6-8. In fact, based on the present results, we would argue that the latter is a direct consequence of the former. For example, in order to explain an ‘extreme’ (relaxed) NCF cluster like 3C 129 on the basis of the results presented in §4, we require an extraordinarily large entropy injection level of  $S_i > 500 \text{ keV cm}^2$  (see Fig. 9). This may seem unlikely, but Fig. 11 indeed demonstrates that 3C 129 has a very high central entropy. Also consistent with this trend are intermediate clusters such as A2589, AWM 4, and A1413 (which lie more or less in the middle of the  $L - T$  and  $L - M$  relations), that show elevated central entropies, and massive “cooling flow” clusters, such as PKS0745 and Hydra A, which show almost no excess entropy in their cores.

So the entropy injection plus cooling model we have proposed works fairly well in terms of explaining the observed entropy profiles of massive clusters. However, the current sample of 11 profiles is obviously too small to be definitive. It should also be noted that the majority of clusters with published entropy profiles were selected on the basis of prior (i.e., *ROSAT/ASCA*) evidence for “cooling flows” (see Figs. 7 & 8). Therefore, it is reasonable to expect that the current data set is biased towards clusters with low central entropies. This may be partially responsible for earlier claims that large amounts of entropy injection are ruled out (e.g., Pratt & Arnaud 2003; Mushotzky et al. 2003). A simple way of testing this model would be to obtain the entropy profiles for a large, *representative* sample of clusters. It should be kept in mind that NCF clusters could make up 30% (or more) of all nearby clusters (Peres et al. 1998). We expect that such samples will soon be available as more and more *Chandra* and *XMM-Newton* data become public.

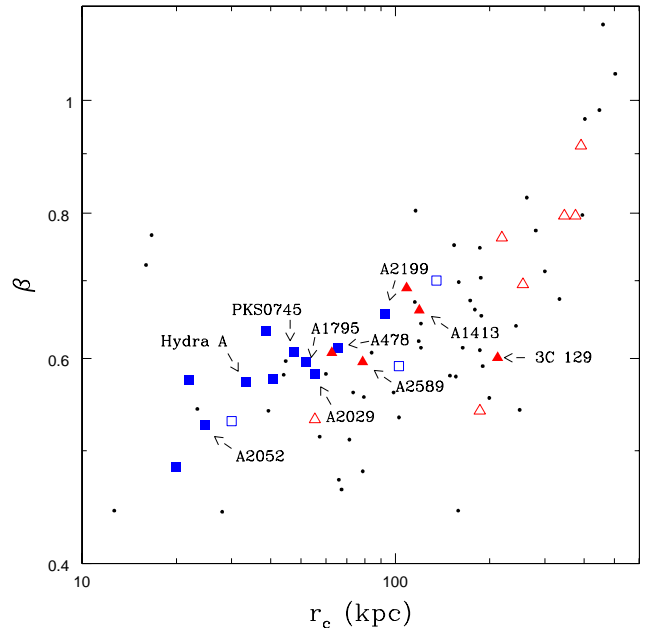


Fig. 12. The  $\beta - r_c$  relation for nearby, massive clusters observed with *ROSAT* by Reiprich & Böhringer (2002). The symbols have the same meaning as in Fig. 7. Labeled clusters are those with published entropy profiles (see Fig. 11).

## 5.2. Surface brightness profiles

X-ray observers often parameterize the observed X-ray surface brightness profiles by fitting the observed profile to assumed analytic functions. The simplest and most commonly used of these is the  $\beta$  model (Cavaliere & Fusco-Femiano 1976). This family of curves is characterized by two parameters:  $r_c$ , which measures the size of the constant surface brightness X-ray core, and  $\beta$ , which measures how rapidly the X-ray flux falls off with radius beyond the core. While we recognize that the simple  $\beta$  model does not provide a perfect match to *either* the observed profiles or the predicted profiles of our model clusters, the approach does provide a useful characterization of the data/models for the purposes of comparison especially since the values of  $\beta$  and  $r_c$  for the observed profiles are readily available in literature.

Plotted in Fig. 12 is the observed relationship between the surface brightness shape parameters,  $\beta$  and  $r_c$ , as determined by Reiprich & Böhringer (2002) by fitting the single  $\beta$  model to clusters in the extended *ROSAT* HIFLUGCS sample. Only those clusters in common with the ACC have been plotted. For clarity, we have not plotted measurement error bars. Typically, measurement uncertainty on  $\beta$  and  $r_c$  is  $\lesssim 10\%$ .

One immediately noticeable trend is that the “cooling flow” and “non-cooling flow” clusters are separated according to core radius size and, to a much lesser extent, by the value of  $\beta$ . This trend between core radius size and “cooling flow” status has been known for some time (e.g., Mohr, Mathiesen, & Evrard 1999; Ota & Mitsuda 2002). More interestingly, the unrelaxed systems (particularly the unrelaxed NCF clusters) appear to be separated from the relaxed systems, in the sense that systems that are undergoing (or have recently undergone) mergers have larger core radii than those systems which

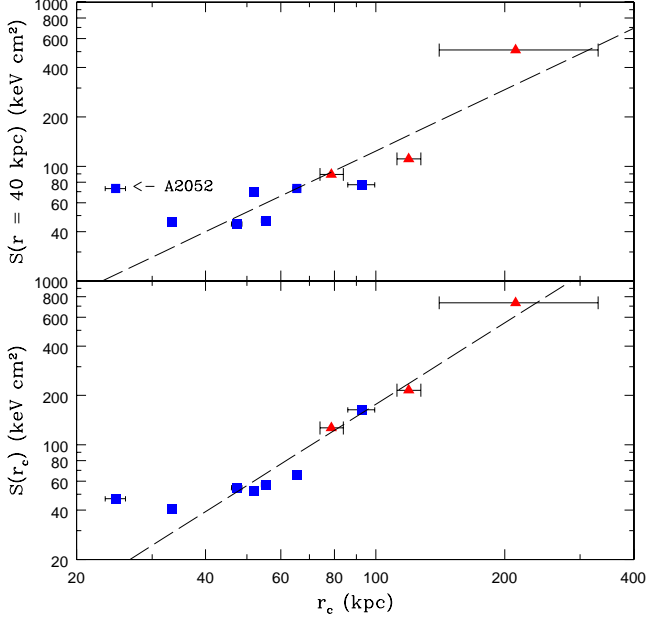


Fig. 13. The observed relationship between core radius size and central entropy for the clusters plotted in Fig. 11. *Top*: Entropy at 40 kpc. *Bottom*: Entropy at the core radius. Measurement uncertainty in the entropy is typically 10%. Symbols have the same meaning as in Fig. 7. Dashed lines indicate the best fit power-laws to the relations (excluding A2052, see text). Namely,  $\log[S(r = 40\text{kpc})] = 1.24 \log r_c - 0.39$  and  $\log[S(r_c)] = 1.65 \log r_c - 1.05$ .

appear relaxed. Given the results of §4.1, therefore, it would seem that mergers tend to influence the structural profiles of clusters (within the central regions) but not the overall global properties. This is consistent with the fact that “cooling flow correction” of relaxed CF clusters results in global properties typical of (relaxed and unrelaxed) NCF clusters (e.g., the “cooling flow corrected”  $L - T$  relation; Markevitch 1998).

In §5.1, we found a correlation between dispersion in the  $L - T$  and  $L - M$  relations and the central entropy of clusters. Comparison of Fig. 12 with Figs. 7 and 8 illustrates that there is also a correlation between dispersion in the scaling relations and the size of a cluster’s core radius. Therefore, we should expect an observed relationship between the size of a cluster’s core radius and its central entropy. These quantities are plotted in Fig. 13 for the *relaxed* clusters explicitly labeled in Figs. 11 and 12. In the top panel of Fig. 13, we plot the entropy at a radius of 40 kpc versus core radius size, while in the bottom panel we plot the entropy at the core radius versus the core radius size.

With the exception of A2052, the results plotted in the top panel of Fig. 13 clearly demonstrate that the core radius of a cluster increases with increasing central entropy. The dashed lines show the best fit power-law relationship between the central entropy and core radius excluding A2052. The bottom panel, which instead plots the entropy at the core radius versus core radius size, shows an even tighter relationship with  $\log S(r_c) = 1.65 \log r_c - 1.05$  (with  $r_c$  in kpc and  $S(r_c)$  in  $\text{keV cm}^2$ ).

A possible explanation for why A2052 is scattered away from the trend traced out by the rest of the clusters in

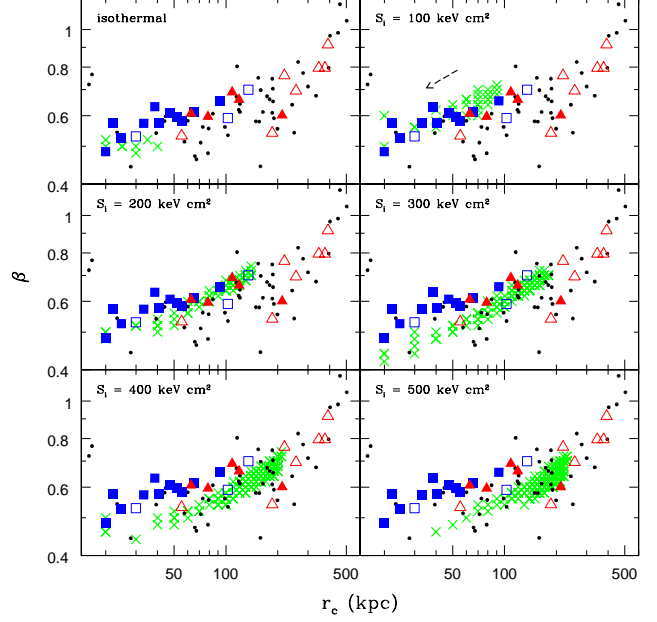


Fig. 14. Comparison of theoretical models to the observed  $\beta - r_c$  relation. The symbols have the same meaning as in Fig. 7 with the exception of the diagonal crosses, which represent the model predictions (see text). The arrow in the upper right hand panel indicates which way the model predictions evolve as the clusters cool.

Figure 13 is the presence of prominent bubbles in the core of this cluster (Blanton et al. 2003). While it is true that a number of other CF clusters plotted in Figure 13 also show evidence for bubbles in central regions (eg. A2199 and Hydra A), the bubbles in these clusters are relatively small compared to size of the region over which the gas is cooling (i.e., region within which the gas temperature declines towards the cluster center). A2052, by contrast, has “large” bubbles and the impact of these features is such that one can account for the “cooling flow” properties of A2052 by azimuthally averaging over the X-ray bright, cool, bubble shells (McCarthy et al. 2003c). We hypothesize that the anomalous values of  $\beta$  and  $r_c$  for A2052 are the result of contamination from these bubbles. This illustrates a potential pitfall of characterizing the surface brightness profiles of clusters with simple  $\beta$  models, in that substructure can potentially throw off the fit to the data and give misleading results. Nonetheless, we find it quite remarkable that, within the context of the small sample we have examined, most systems follow a tight trend between core radius size and central entropy.

It is interesting to see whether or not the models can explain the  $\beta - r_c$  relation plotted in Fig. 12 and also account for the relationship between the central entropy and  $r_c$  as well. Plotted in Fig. 14 is a comparison of the observed and predicted  $\beta - r_c$  relations. The symbols have the same meaning as in Fig. 7 with exception of the diagonal crosses, which represent the model predictions. The crosses are the result of fitting single  $\beta$  models to the model surface brightness profiles as a function of time (as the cluster cools) for a suitable range of cluster masses [i.e.,  $M(r_{500}) \gtrsim 10^{14} M_\odot$ ]. As the clusters cool, both  $\beta$  and (especially)  $r_c$  decrease (i.e., with time, the model

predictions typically move from upper right hand side of the plot to the lower left hand side; see arrow in upper right hand panel).

The results of Fig. 14 illustrate that models with entropy injection levels of  $S_i \lesssim 200 \text{ keV cm}^2$  + radiative cooling can account for relaxed CF clusters, while higher levels of entropy injection are typically required to explain relaxed NCF clusters. This is in excellent agreement with the results of §5. Not surprisingly, the unrelaxed NCF systems have core radii that are much larger than can be accounted for by the model clusters (which, by definition, are relaxed). Therefore, core radius size is a potentially promising way of distinguishing between relaxed and unrelaxed systems. In addition, the crosses in Fig. 14 indicate that as one injects more and more entropy into a system the larger its core becomes (as is also evident from Figs. 2 and 3). This qualitatively matches the trends seen in Fig. 13. Because the central entropy and core radius evolve with time in the models, a more direct comparison between theory and observations would require knowledge about how long each observed system has been able to cool for.

### 5.3. Temperature profiles

Finally, we make a comparison between observed and predicted temperature profiles. Plotted in Fig. 15 is the so-called universal temperature profile of Allen, Schmidt, & Fabian (2001). This was derived from a sample of 6 clusters observed with *Chandra* and classified as relaxed, massive “cooling flow” clusters by these authors. Also shown (solid lines) are the predictions of our entropy injection plus cooling model *after the initial core has dropped out* for a range of cluster masses. The model profiles have been normalized the same way as the observational results; i.e., radii have been normalized to  $r_{2500}$  and temperatures have been normalized to the temperature at that radius.

Overall, the fit to observational data is quite good. There is a hint of some slight differences at very small radii, although the hatched region (which represents Allen, Schmidt, & Fabian’s best fit to their data) does not encompass all of the scatter in the observed temperature profiles (see Fig. 1 of Allen, Schmidt, & Fabian 2001). Thus, so long as there is enough time to cool out the initial entropy core, the model does a very good job of matching relaxed, massive CF clusters.

Unfortunately, there are very few relaxed NCF clusters with published *Chandra* or *XMM-Newton* temperature profiles. Furthermore, comparison with observations is made difficult by the fact that our model does not predict a quasi-steady state “non-cooling flow” temperature profile but, rather, a full distribution of profiles (see Fig. 4). We do note, however, that 3C 129 has a sharp *negative* temperature gradient at its center (i.e., sharp rise towards the center; see Fig. 2 of Krawczynski 2002), which is qualitatively what we should expect from a system that had a large injection of entropy (see Fig. 4).

## 6. DISCUSSION

A major result of the present study is that a relatively wide range in entropy injection levels combined with subsequent radiative cooling is required to explain the observed global and structural properties of massive clusters. That cooling is an essential process is the least

surprising result. The very fact that clusters are radiating in X-rays is evidence that they are cooling. However, the large scatter in their global and structural properties suggests large cluster-to-cluster variations in cooling efficiency. We have shown that this can be accounted for as a by-product of variations in the level of entropy injection. Regardless of the source of the entropy injection, cluster-to-cluster variations in injection efficiency are to be expected. A similar suggestion was recently put forward by Sun et al. (2003b) in order to explain scatter in the observed entropy profiles of 6 low mass groups.

Variations in the injection level can also naturally account for the dichotomy between NCF and CF clusters. The prevailing view is that NCF clusters are systems that have been disrupted by recent major mergers. This picture is often supported by images of NCF clusters which show disturbed X-ray morphologies (although, admittedly, NCF clusters typically have flatter surface brightness profiles and, therefore, it should be easier to pick out irregularities in these systems than in CF clusters). Indeed, it is likely that some of the NCFs are the result of mergers, and such systems should be removed from consideration<sup>9</sup>, but, as we have already discussed, there

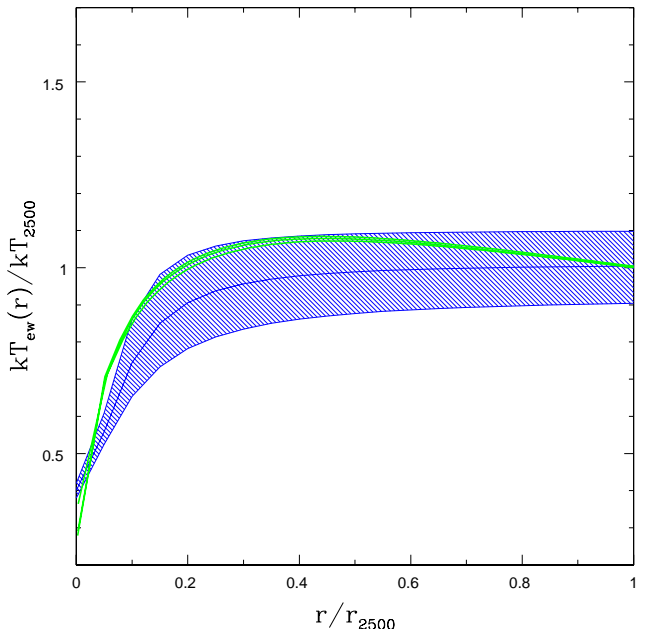


Fig. 15. Comparison of observed and predicted temperature profiles for “cooling flow” clusters. The hatched region represents the observational results of Allen, Schmidt, & Fabian (2001) from a sample of 6 massive, “cooling flow” clusters. The solid black lines represent the predictions of our model *after the entropy core has dropped out* for a range of high mass clusters.

<sup>9</sup> Since only a small fraction of the clusters examined in the present study have high quality *Chandra* or *XMM-Newton* images available, we have not explicitly excluded merger systems from the first part of this study. As we have shown, mergers do not seem to significantly influence *global* properties such as the  $L - T$  and  $L - M$  relations (see §4.1) and, therefore, we do not expect a significant bias to be present. When investigating *structural* properties (§5), on the other hand, only the profiles of relaxed systems were considered, as azimuthally-averaged profiles for highly asymmetric (merging) clusters are essentially meaningless.

are several NCF clusters that look remarkably relaxed and do not show any obvious signs of ongoing mergers (e.g., 3C 129, A2589, A1060, A1651, A1689, AWM 4, A3571, A1413, RX J1200.8-0328, RX J1120.1+4318). Such systems need to be accounted for. Moreover, in the currently favored hierarchical model for structure formation, *all massive systems* are formed through mergers and accretion of smaller objects. Therefore, CF clusters should also experience major mergers, since they are a ubiquitous feature of the  $\Lambda$ CDM cosmology. In fact, Loken, Melott, & Miller (1999) showed that CF clusters tend to occupy more crowded regions of the universe than NCF clusters. Perseus, RX J1347.5-1145, A2142, A1644, and A644 are all examples of clusters which are believed to be undergoing mergers (or have recently undergone a merger) and yet have retained their “cooling flow” identity. This argues against merging being the only difference between CF and NCF clusters.

In order to explore these ideas more explicitly, we have carried out a series of numerical simulation experiments involving the merging of clusters of various mass ratios and impact parameters. In addition, the effects of radiative cooling have been included. The results of this study will be presented in a forthcoming paper (Poole et al. in preparation). We briefly note, however, that the recent hydrodynamic study of Motl et al. (2004) shows that it is extremely difficult to disrupt the dense cores of cooling clusters and, subsequently, form a system that resembles a NCF cluster. Typically, the clusters regain their CF status on a very short time scale. Similar conclusions were reached by Gómez et al. (2002). This lends further credence to the hypothesis that some other mechanism, in addition to merging, may be required in order to explain the relatively large fraction of NCF clusters observed in the local universe. Based on the results of the current study, we would argue entropy injection is the required mechanism.

But what is the source of the additional entropy? This is perhaps the single most important outstanding issue of models which implement entropy injection. A whole host of entropy injection mechanisms (a number of which are discussed in detail in §1 of Babul et al. 2002) have been proposed to explain the overcooling/cooling flow problem and also the global X-ray scaling relations of clusters. The most commonly proposed mechanism is galactic winds driven by supernovae, which are expected to transfer relatively large amounts of thermal energy into the ICM (e.g., Loewenstein 2000; Voit & Bryan 2001). However, in order to explain the scaling relations of clusters, the efficiency of the supernovae must be extremely high (probably unreasonably high) and even then one requires a top-heavy stellar initial mass function (e.g., Balogh et al. 1999; Valageas & Silk 1999). As such, supernovae by themselves are unlikely to be the source of the entropy/energy injection. Heating via quasars and active galactic nuclei (AGN), either prior to or following cluster formation, is a currently popular (proposed) mechanism, since such objects potentially contain vast reservoirs of energy. While it seems there is plenty of energy available, it is still unclear exactly how the AGN heat the gas. Possibilities include Compton heating of intracluster electrons via high energy UV and X-ray photons emitted by the AGN accretion disk (e.g., Ciotti & Ostriker 1997, 2001), shock heating by

transonic or supersonic jets (e.g., Binney & Tabor 1995; Omma et al. 2004), entrainment, transport, and subsequent mixing of low entropy gas via buoyantly rising bubbles of hot plasma inflated by the AGN (e.g., Quilis, Bower, & Balogh 2001; Mathews et al. 2003; Dalla Vecchia et al. 2004), and viscous dissipation of the kinetic energy of the rising bubbles (e.g., Fabian et al. 2003; Ruszkowski, Bruggen, & Begelman 2004). Detailed calculations, which are beyond the scope of this paper, are required in order to assess whether AGN are able to give rise to the distribution of entropy injection levels required to account for the X-ray properties discussed above.

Entropy injection into the central regions of the clusters can also be achieved via heat transport from outer regions. Two transport mechanisms have been proposed: thermal conduction (e.g. Narayan & Medvedev 2001) and turbulent mixing (e.g. Kim & Narayan 2003). Until recently it was thought that conduction would be an inefficient heat transport mechanism, since the presence of intracluster magnetic fields should strongly suppress conduction. However, Narayan & Medvedev (2001) demonstrated that if the magnetic fields are tangled it is still possible to achieve conductivities of up to one-third the Spitzer conductivity. Zakamska & Narayan (2003) subsequently demonstrated with simple models that conduction could offset radiative losses in some (but not all) CF clusters. However, through the use of hydrodynamical simulations that include radiative cooling and conduction, Dolag et al. (2004) showed that while conduction may be important for the most massive clusters, it does not significantly modify the properties of lower mass clusters (since the conductivity has a strong temperature dependence). Thus, thermal conduction is unlikely to be solely responsible for the distribution of entropy injection levels inferred in the present study. On the other hand, turbulent mixing of the intracluster gas, which is likely caused by stirring due to infalling and orbiting substructure, is perhaps more promising (El-Zant et al. 2004; Bildfell et al. in preparation). For example, Kim & Narayan (2003) have demonstrated that one can reproduce the slope of the  $L - T$  relation for high mass clusters with a simple mixing model. However, it has yet to be demonstrated whether such a model can account for the normalization of the relation and its associated scatter.

Finally, we note that our estimates for the amount of non-gravitational entropy required to explain the observed x-ray properties of relaxed clusters — and our subsequent evaluation of the possible sources of this entropy — implicitly assumed that in the absence of any entropy injection, the cluster gas will exhibit a very small entropy core, if any. The reason for making this assumption is because if one places isothermal gas in the cluster potential well (i.e., the standard model), the gas density distribution will have an exponential form and, correspondingly, the entropy profile will have a small core (both in size and amplitude). This implicitly assumes the underlying (dark matter) potential is similar to those found from high resolution numerical simulations. For a singular isothermal sphere, there is no entropy core whatsoever.

The above analytic result is borne out by SPH non-radiative simulations of galaxy clusters. Although there is some evidence for an entropy core in low resolution

simulations, this core decreases in size and amplitude with increasing resolution (e.g., Frenk et al. 1999; Lewis et al. 2000), indicating that the core in the low-resolution simulations is a numerical artifact.

More recently, though, high-resolution mesh-based (e.g., AMR) non-radiative simulations show substantial entropy cores that persist even when the simulation resolution is increased, while agreeing with SPH results at large radii (e.g., Voit et al. 2003). Moreover, there appears to be a coupling between the magnitude and the size of the entropy core in individual cluster and the cluster’s merger history. The origin of the core, and in fact whether the core is indeed real has yet to be ascertained. In fact, there is no clear explanation available as to why the SPH and mesh-based codes give such different result. Clearly, though, a more careful study is warranted because if the AMR results are correct, then the stringent constraints on the amount of non-gravitational entropy injection required is correspondingly reduced. Quite independent of how the entropy core arises, our present study demonstrates that a distribution in magnitudes of the central entropy cores in galaxy clusters is key to understanding their global and structural properties.

Finally, in the present study, we have purposely focused on high mass clusters since temperatures and luminosities are fairly straightforward quantities to measure for these systems. However, a complete picture must also address the intragroup medium. The low X-ray luminosity of poor groups makes this a difficult challenge. Not only are there much poorer statistics, in terms of low signal-to-noise ratios, but a significant fraction of the flux can originate from point sources and the ISM of the central galaxy, making disentanglement of the ICM that much harder. A good example of just how difficult it is to obtain reliable results from group data is presented in the recent study of Osmond & Ponman (2004). By simply increasing the number of low temperature systems in their data set, and also correcting the luminosity to a fixed overdensity, these authors found that the evidence for steepening of the  $L-T$  relation in groups (e.g., Mulchaey & Zabludoff 1998; Helsdon & Ponman 2000), relative to self-similar predictions, is no longer solid. In order to make a fair comparison between the models and group data, one needs to fold the instrumental response of the X-ray satellite into the theoretical models. Furthermore, the models should be analysed the same way as the observational data (Poole et al. 2004b in preparation). A future project, therefore, is to ‘observe’, with a mock X-ray satellite (which mimics *Chandra* or *XMM-Newton*), a realistic population of groups and clusters that includes the effects of radiative cooling and specific entropy injection processes such as conduction, mixing, and AGN heating.

## 7. CONCLUSIONS

Recent X-ray observations have highlighted the lack of large isentropic cores in groups and clusters and have led some to suggest that radiative cooling is the dominant mechanism in the breaking of self-similarity. However, radiative cooling alone leads to a predicted overabundance of cooled gas in theoretical models (the so-called “cooling crisis”). In order to explain the observed entropy profiles and also retain consistency with the observed fraction of cold baryons (stars) in clusters, it is

likely that both radiative cooling and some form of entropy injection are required. We have performed a thorough investigation of this scenario by adding a realistic treatment of the effects of radiative cooling to the entropy injection model of Babul et al. (2002). A comparison to the current suite of X-ray observations was then made with a particular emphasis on assessing whether or not the model could account for the large amount of intrinsic scatter in the observed scaling relations and, simultaneously, account for the observed entropy, surface brightness, and temperature profiles of clusters. The main results can be summarized as follows:

- Injecting the ICM with  $S_i \gtrsim 200 \text{ keV cm}^2$  prevents significant mass drop out due to radiative cooling and insures the observed fraction of cold baryons ( $\lesssim 10\%$ ; Balogh et al. 2001) is not violated.
- Radiative cooling approximately maintains the initial power-law between entropy and radius,  $S \propto r^{1.1}$ , at large radii and extends it to small radii as well, so long as there is enough time for cooling to wash out the effects of any non-gravitational entropy injection.
- Depending on the time elapsed since entropy injection (i.e., the time available for the cluster to cool radiatively), the model naturally predicts either clusters with flat central surface brightnesses and sharp central negative temperature gradients or clusters with peaked surface brightnesses and central positive temperature gradients. These match the main qualitative features of NCF and CF clusters, respectively.
- Radiative cooling tends to have a larger effect on the luminosity of a cluster than its temperature. So long as only a small fraction of the cluster’s baryons are cooled out ( $\lesssim 10\%$ ), the result is that cooling moves the predicted  $L-T$  relation to higher luminosities at a fixed temperature.
- An analysis of the  $L-T$  and  $L-M$  relations derived from the ACC of Horner (2001) and the extended HIFLUGCS of Reiprich & Böhringer (2002) demonstrates that there is a strong correlation between dispersion in these relations and “cooling flow” status. Although this trend has been illustrated before for the  $L-T$  relation (although probably not as clearly), this is the first time it has been demonstrated for the  $L-M$  relation.
- We find that a distribution of entropy injection levels combined with the effects of radiative cooling can account for the observed  $L-T$  and  $L-M$  relations and the large amount of intrinsic scatter associated with each. This is the first time a theoretical model has been shown to account for this intrinsic scatter. We also find that so-called “cooling flow” clusters typically require ‘mild’ amounts of entropy injection ( $S_i \lesssim 300 \text{ keV cm}^2$ ), whereas “non-cooling flow” clusters require larger amounts of injection. Interestingly, this dividing line is essentially equal to the cooling threshold for massive clusters (Voit & Bryan 2001; Babul et al. 2002),



implying that the amount of entropy injection dictates which class (CF or NCF) a particular cluster will fall under. Moreover, so long as the CF clusters were injected with  $S_i \gtrsim 200 \text{ keV cm}^2$ , their predicted cold gas fractions do not violate observational constraints.

- A natural consequence of our explanation for the scatter of the  $L-T$  and  $L-M$  relations is that the central entropy of clusters should increase as one goes from the high-luminosity side of these scaling relations to the low-luminosity side. An examination of the deprojected entropy profiles of 11 relaxed massive CF and NCF systems observed with *Chandra* and/or *XMM-Newton* reveals just such a correlation between central entropy and dispersion in these scaling relations. It is this trend which likely gives rise to the previously identified relationship between  $L-T$  dispersion and inferred cooling flow strength (see Fabian et al. 1994).
- The model predicts surface brightness profiles that are consistent with those of relaxed CF clusters when mild amounts of entropy are injected ( $S_i \lesssim 200 \text{ keV cm}^2$ ) and with relaxed NCF clusters when higher amounts of entropy are injected. This is in good agreement with the constraints placed on  $S_i$  from analysis of the  $L-T$  and  $L-M$  relations. The model also qualitatively explains the observed (newly discovered) relationship between a cluster's central entropy and the size of its core radius.
- We demonstrate that the model can also successfully explain the observed universal temperature profile (for relaxed, massive CF clusters) of Allen, Schmidt, & Fabian (2001).

- At present, there is a dearth of structural information (e.g., entropy and temperature profiles) of relaxed NCF clusters from *Chandra* and *XMM-Newton* data. A large number of the NCF clusters observed with these satellites are the sites of ongoing mergers (e.g., Govoni et al. 2004). It is important to note, however, that in most cases *these clusters were selected because they were known to be mergers* (for the purposes of studying ‘cold fronts’, bow shocks, etc.). However, there are examples of relaxed NCF clusters observed previously with *ROSAT* and *ASCA* (e.g., Buote & Tsai 1996, see also §6 of the present study). A simple way of testing the present model, therefore, would be to obtain deprojected entropy profiles for these systems (using the current generation of satellites) and see whether or not they possess elevated entropy levels at the centers.

The authors wish to thank the referee for useful comments which improved the quality of the paper, particularly the discussion of observational results. We thank Alastair Edge, Gilbert Holder, James Binney, and Greg Bryan for useful comments on an earlier version of the manuscript. We also thank Steve Allen, Roderick Johnstone, Henric Krawczynski, Ewan O’Sullivan, and Ming Sun for providing their *Chandra*/*XMM-Newton* results in electronic form and Greg Bryan and Mark Voit for providing the entropy profiles of their numerically simulated clusters. I. G. M. is supported by a postgraduate scholarship from Natural Sciences and Engineering Research Council of Canada (NSERC). A. B. is supported by an NSERC Discovery Grant and M. L. B. is supported by a PPARC fellowship.

## REFERENCES

- Allen, S. W., & Fabian, A. C. 1998, *MNRAS*, 297, L57  
 Allen, S. W., Schmidt, R. W., & Fabian A. C. 2001, *MNRAS*, 328, L37  
 Allen, S. W., Schmidt, R. W., & Fabian A. C. 2002, *MNRAS*, 335, 256  
 Babul, A., Balogh, M. L., Lewis, G. F., & Poole, G. B. 2002, *MNRAS*, 330, 329  
 Balogh, M. L., Babul, A., & Patton, D. R. 1999, *MNRAS* 307, 463  
 Balogh, M. L., Babul, A., Voit, G. M., McCarthy, I. G., Jones, L. R., Lewis, G. F., & Ebeling, H. 2004, *MNRAS*, submitted  
 Balogh, M. L., Pearce, F. R., Bower, R. G., and Kay, S. T. 2001, *MNRAS*, 326, 1228  
 Bauer, F., & Sarazin, C. L. 2000, *ApJ*, 530, 222  
 Benson, A. J., Bower, R. G., Frenk, C. S., Lacey, C. G., Baugh, C. M., & Cole, S. 2003, *ApJ*, 599, 38  
 Binney, J., & Tabor, G. 1995, *MNRAS*, 276, 663  
 Blanton, E. L., Sarazin, C. L., & McNamara, B. R. 2003, *ApJ*, 585, 227  
 Borgani, S., Governato, F., Wadsley, J., Menci, N., Tozzi, P., Lake, G., Quinn, T., & Stadel, J. 2001, *ApJ*, 559, L71  
 Bryan, G. L. 2000, *ApJ*, 544, L1  
 Buote, D. A., & Lewis, A. D. 2004, *ApJ*, 604, 116  
 Buote, D. A., & Tsai, J. C. 1996, *ApJ*, 458, 27  
 Cavaliere, A., & Fusco-Femiano, R. 1976, *A&A*, 49, 137  
 Chen, Y., Ikebe, Y., Böhringer, H. 2003, *A&A*, 407, 41  
 Ciotti, L., & Ostriker J. P. 1997, *ApJ*, 487, L105  
 —. 2001, *ApJ*, 551, 131  
 Cole, S., et al. 2001, *MNRAS*, 326, 255  
 Dalla Vecchia, C., Bower, R., Theuns, T., Balogh, M. L., Mazzotta, P., & Frenk, C. S. 2004, *MNRAS*, submitted  
 Davé, R., Katz, N., & Weinberg, D. H. 2002, *ApJ*, 579, 23  
 David, L. P., Nulsen, P. E. J., McNamara, B. R., Forman, W., Jones, C., Ponman T., Robertson, B., & Wise, M. 2001, *ApJ*, 557, 546  
 De Grandi, S., & Molendi, S. 2002, *ApJ*, 567, 163  
 Dolag, K., Jubelgas, M., Springel, V., Borgani, S., & Rasia, E. 2004, *ApJ*, 606, L97  
 Donahue, M., Mack, J., Voit, G. M., Sparks, W., Elston, R., & Maloney, P. R. 2000, *ApJ*, 545, 670  
 Dupke, R., & White, R. E., III 2003, 583, L13  
 Edge, A. C. 2001, *MNRAS*, 328, 762  
 Edge, A. C., Wilman, R. J., Johnstone, R. M., Crawford, C. S., Fabian, A. C., & Allen, S. W. 2002, *MNRAS*, 337, 49  
 El-Zant, A., Kim, W.-T., & Kamionkowski, M. 2004, *MNRAS*, submitted (astro-ph/0403696).  
 Ettori, S., Fabian, A. C., Allen, S. W., & Johnstone, R. M. 2002, *MNRAS*, 331, 635  
 Evrard, A. E., Metzler, C. A., & Navarro, J. F. 1996, *ApJ*, 469, 494  
 Fabian, A. C., Crawford, C. S., Edge, A. C., & Mushotzky, R. F. 1994, *MNRAS*, 267, 779  
 Fabian, A. C., Sanders, J. S., Allen, S. W., Crawford, C. S., Iwasawa, K., Johnstone, R. M., Schmidt, R. W., & Taylor, G. B. 2003, *MNRAS*, 344, L43  
 Frenk, C. S., White, S. D. M., Bode, P., Bond, J. R., Bryan, G. L., Cen, R., Couchman, H. M. P., Evrard, A. E., Gnedin, N., Jenkins, A., Khokhlov, A. M., Klypin, A., Navarro, J. F., Norman, M. L., Ostriker, J. P., Owen, J. M., Pearce, F. R., Pen, U.-L., Steinmetz, M., Thomas, P. A., Villumsen, J. V., Wadsley, J. W., Warren, M. S., Xu, G., & Yepes, G. 1999, *ApJ*, 525, 554  
 Fujita, Y., Sarazin, C. L., Kempner, J. C., Rudnick, L., Slee, O. B., Roy, A. L., Andernach, H., Ehle, M. 2002, *ApJ*, 575, 764  
 Gómez, P. L., Loken, C., Roettiger, K., & Burns, J. O. 2002, *ApJ*, 569, 122  
 Govoni, F., Markevitch, M., Vikhlinin, A., Van Speybroeck, L., Feretti, L., and Giovannini, G. 2004, *ApJ*, 605, 695

- Gutierrez, K., & Krawczynski, H. 2003, ApJ, submitted (astro-ph/0312454)
- Helsdon, S. F., & Ponman, T. J. 2000, MNRAS, 315, 356
- Henriksen, M. J., & Tittley, E. R. 2002, ApJ, 577, 701
- Horner, D. J. 2001, PhD Thesis, University of Maryland
- Johnstone, R. M., Allen, S. W., Fabian, A. C., & Sanders, J. S. 2002 MNRAS, 336, 299
- Kaastra, J. S., Tamura, T., Peterson, J. R., Bleeker, J. A. M., Ferrigno, C., Kahn, S. M., Paerels, F. B. S., Piffaretti, R., Branduardi-Raymont, G., & Böhringer, H. 2004, A&A, 413, 415
- Kaiser, C. R., & Binney, J. 2003, MNRAS, 338, 837
- Kaiser, N. 1991, ApJ, 383, 104
- Kempner, J. C., Sarazin, C. L., & Markevitch, M. 2003, ApJ, 593, 291
- Kempner, J. C., Sarazin, C. L., & Ricker, P. M. 2002, ApJ, 579, 236
- Kim, W. T., & Narayan, R. 2003, ApJ, 596, L139
- Krawczynski, H. 2002, ApJ, 569, L27
- Lewis, A. D., & Buote, D. A. 2002, in American Physical Society, April Meeting, Jointly Sponsored with the High Energy Astrophysics Division (HEAD) of the American Astronomical Society April 20 - 23, 2002 Albuquerque Convention Center Albuquerque, New Mexico
- Lewis, A. D., Buote, D. A., & Stocke, J. T. 2003, ApJ, 586, L135
- Lewis, G. F., Babul, A., Katz, N., Quinn, T., Hernquist, L., & Weinberg, D. H. 2000, ApJ, 536, 623
- Lin, Y. T., Mohr, J. J., & Stanford, S. A. 2003, ApJ, 591, 749
- Loewenstein, M. 2000, ApJ, 532, 17
- Loken, C., Melott, A. L., & Miller, C. J. 1999, ApJ, 520, L5
- Loken, C., Norman, M. L., Nelson, E., Burns, J., Bryan, G. L., & Motl, P. 2002, ApJ, 579, 571
- Machacek, M. E., Bautz, M. W., Canizares, C., & Garmire, G. P. 2002, ApJ, 567, 188
- Markevitch, M. 1998, ApJ, 504, 27
- Markevitch, M., Ponman, T. J., Nulsen, P. E. J., Bautz, M. W., Burke, D. J., David, L. P., Davis, D., Donnelly, R. H., Forman, W. R., Jones, C., Kaastra, J., Kellogg, E., Kim, D.-W., Kolodziejczak, J., Mazzotta, P., Pagliaro, A., Patel, S., Van Speybroeck, L., Vikhlinin, A., Vrtilek, J., Wise, M., & Zhao, P. 2000, ApJ, 541, 542
- Markevitch, M., & Vikhlinin, A. 2001, ApJ, 563, 95
- Mathews, W. G., Brighenti, F., Buote, D. A., & Lewis, A. D. 2003, ApJ, 596, 159
- Mazzotta, P., Edge, A. C., Markevitch, M. 2003, ApJ, 596, 190
- Mazzotta, P., Fusco-Femiano, R., & Vikhlinin, A. 2002, ApJ, 569, L31
- Mazzotta, P., Markevitch, M., Vikhlinin, A., Forman, W. R., David, L. P., & Van Speybroeck, L. 2001, 555, 205
- McCarthy, I. G., Babul, A., & Balogh, M. L. 2002a, ApJ, 573, 515
- McCarthy, I. G., Babul, A., Holder, G. P., & Balogh, M. L. 2003a, ApJ, 591, 515
- McCarthy, I. G., Babul, A., Katz, N., & Balogh, M. L. 2003c, ApJ, 587, L75
- McCarthy, I. G., Holder, G. P., Babul, A., & Balogh, M. L. 2003b, ApJ, 591, 526
- McCarthy, I. G., West, M. J., & Welch, G. A. 2002b, ApJ, 567, 762
- McNamara, B. R., Wise, M. W., Nulsen, P. E. J., David, L. P., Carilli, C. L., Sarazin, C. L., O'Dea, C. P., Houck, J., Donahue, M., Baum, S., Voit, M., O'Connell, R. W., & Koekemoer, A. 2001, ApJ, 562, L149
- Mohr, J. J., Mathiesen, B., & Evrard, A. E. 1999, ApJ, 517, 627
- Moore, B., Ghigna, S., Governato, F., Lake, G., Quinn, T., Stadel, J., & Tozzi, P. 1999, ApJ, 524, L19
- Motl, P. M., Burns, J. O., Loken, C., Norman, M. L., & Bryan, G. L. 2004, ApJ, in press
- Muanwong, O., Thomas, P. A., Kay, S. T., and Pearce, F. R. 2002, MNRAS, 336, 527
- Mulchaey, J. S., & Zabludoff, A. I. 1998, ApJ, 496, 73
- Mushotzky, R., Figueroa-Feliciano, E., Loewenstein, M., & Snowden, S. L. 2003, ApJ, submitted (astro-ph/0302267)
- Narayan, R., & Medvedev, M. V. 2001, ApJ, 562, L129
- Novicki, M. C., Sornig, M., & Henry, J. P. 2002, AJ, 124, 2413
- Oh, S. P., & Benson, A. J. 2003, MNRAS, 342, 664
- Omma, H., Binney, J., Bryan, G., & Slyz, A. 2004, MNRAS, 348, 1105
- Osmond, J. P. F., & Ponman, T. J. 2003, MNRAS, submitted
- O'Sullivan, E., & Vrtilek, J. M. 2003, in The Riddle of Cooling Flows in Galaxies and Clusters of Galaxies, ed. T. Reiprich, J. Kempner, & N. Soker, published electronically at <http://www.astro.virginia.edu/coolflow/>
- Ota, N., & Mitsuda, K. 2002, ApJ, 567, L230
- Peres, C. B., Fabian, A. C., Edge, A. C., Allen, S. W., Johnstone, R. M., & White, D. A. 1998, MNRAS, 298, 416
- Peterson, J. R., Paerels, F. B. S., Kaastra, J. S., Arnaud, M., Reiprich, T. H., Fabian, A. C., Mushotzky, R. F., Jernigan, J. G., & Sakellou, I. 2001, A&A, 365, L104
- Peterson, J. R., Kahn, S. M., Paerels, F. B. S., Kaastra, J. S., Tamura, T., Bleeker, J. A. M., Ferrigno, C., & Jernigan, J. G. 2003, ApJ, 590, 207
- Pratt, G. W., & Arnaud, M. 2002, A&A, 394, 375
- Pratt, G. W., & Arnaud, M. 2003, A&A, 408, 1
- Quilis, V., Bower, R. G., & Balogh, M. L. 2001, MNRAS, 328, 1091
- Reiprich, T. H., & Böhringer, H. 2002, ApJ, 567, 716
- Ruszkowski, M., Bruggen, M., & Begelman, M. C. 2004, ApJ submitted (astro-ph/0403690)
- Sauvageot, J. L., Belsole, E., Arnaud, M., & Ponman, T. J. 2001, in Clusters of galaxies and the high redshift universe observed in X-rays, Recent results of XMM-Newton and Chandra, ed. D. M. Neumann, & J. T. T. Van, published electronically at [http://www-dapnia.cea.fr/Conferences/Morion\\_astro\\_2001/index.html](http://www-dapnia.cea.fr/Conferences/Morion_astro_2001/index.html)
- Scannapieco, E., & Oh, S. P. 2004, ApJ, submitted (astro-ph/0401087)
- Scharf, C. A., & Mushotzky, R. F. 1997, 485, L65
- Schmidt, R. W., Allen, S. W., & Fabian, A. C. 2001, MNRAS, 327, 1057
- Smith, G. P., Edge, A. C., Eke, V. R., Nichol, R. C., Smail, I., & Kneib, J.-P. 2003, ApJ, 590, L79
- Somerville, R., & Primack, J. R. 1999, MNRAS, 310, 1087
- Spergel, D. N., Verde, L., Peiris, H. V., Komatsu, E., Nolte, M. R., Bennett, C. L., Halpern, M., Hinshaw, G., Jarosik, N., Kogut, A., Limon, M., Meyer, S. S., Page, L., Tucker, G. S., Weiland, J. L., Wollack, E., & Wright, E. L. 2003, ApJS, 148, 175
- Sun, M., Forman, W., Vikhlinin, A., Hornstrup, A., Jones, C., & Murray, S. S. 2003b, ApJ, 598, 250
- Sun, M., Jones, C., Murray, S. S., Allen, S. W., Fabian, A. C., & Edge, A. C. 2003a, ApJ, 587, 619
- Sun, M., & Murray, S. S. 2002, ApJ, 576, 708
- Sun, M., Murray, S. S., Markevitch, M., & Vikhlinin, A. 2002, ApJ, 565, 867
- Takizawa, M., Sarazin, C. L., Blanton, E. L., & Taylor, G. B. 2003, ApJ, 595, 142
- Tozzi, P., & Norman, C. 2001, ApJ, 546, 63
- Valageas, P., & Silk, J. 1999, A&A, 350, 725
- Voit, G. M., & Bryan, G. L. 2001, Nature, 414, 425
- Voit, G. M., Bryan, G. L., Balogh, M. L., & Bower, R. G. 2002, ApJ, 576, 601
- Voit, G. M., Balogh, M. L., Bower, R. G., Lacey, C. G., & Bryan, G. L. 2003, ApJ, 593, 272
- Voit, G. M., & Ponman, T. J. 2003, ApJ, 549, L75
- White, D. A., Jones, C., & Forman, W. 1997, MNRAS, 292, 419
- Wise, M. W., McNamara, B. R., & Murray, S. S. 2004, ApJ, 601, 184
- Wu, X., & Xue, Y. 2002, ApJ, 572, L19
- Xue, S.-J., & Wu, X.-P. 2002, ApJ, 576, 152
- Yamasaki, N. Y., Ohashi, T., & Furusho, T. 2002, ApJ, 578, 833
- Yoshida, N., Stoehr, F., Springel, V., & White, S. D. M. 2002, MNRAS, 335, 762
- Zakamska, N. L., & Narayan, R. 2003, ApJ, 582, 162